








CPT1C is required for synaptic plasticity and oscillatory activity that supports motor, associative and non-associative learning

Guillermo Iborra-Lázaro¹ , Souhail Djebari¹ , Irene Sánchez-Rodríguez¹, Esther Gratacòs-Batlle^{2,3} , Nuria Sánchez-Fernández², Marija Radošević³, Núria Casals⁴ , Juan de Dios Navarro-López¹ , David Soto del Cerro^{2,3}  and Lydia Jiménez-Díaz¹ 

¹Neurophysiology & Behaviour Laboratory, Regional Centre for Biomedical Research (CRIB), Faculty of Medicine of Ciudad Real, University of Castilla-La Mancha, Ciudad Real, Spain

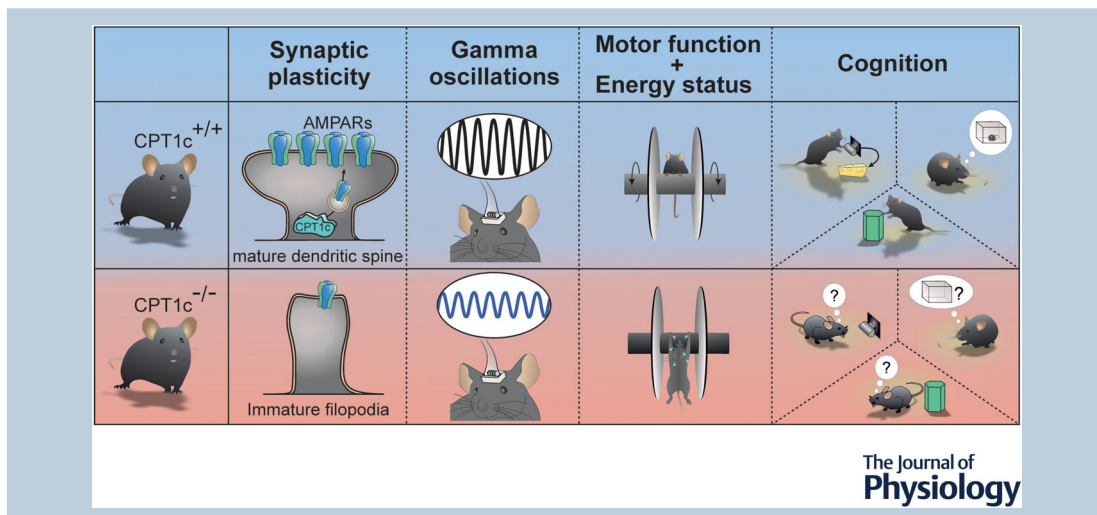
²Laboratory of Neurophysiology, Department of Biomedicine, Faculty of Medicine and Health Sciences, Institute of Neurosciences, University of Barcelona, Barcelona, Spain

³August Pi i Sunyer Biomedical Research Institute (IDIBAPS), Barcelona, Spain

⁴Basic Sciences Department, Faculty of Medicine and Health Sciences, Universitat Internacional de Catalunya and Centro de Investigación Biomédica en Red de Fisiopatología de la Obesidad y la Nutrición (CIBEROBN), Instituto de Salud Carlos III, Barcelona, Spain

Handling Editors: David Wyllie & James Coxon

The peer review history is available in the Supporting information section of this article (<https://doi.org/10.1113/JP284248#support-information-section>).



Guillermo Iborra-Lázaro After he graduated in Biology at the University of Alicante (2017), Iborra-Lázaro completed a Master's degree in Neuroscience (2018) while conducting a Master's Research Project focused on the molecular mechanisms underlying Alzheimer's disease. Afterwards, as a predoctoral researcher in the Laboratory of Neurophysiology and Behaviour at the Faculty of Medicine of Ciudad Real, he studied the role of the CPT1C protein in the nervous system and the mechanisms altered in early stages of Alzheimer's disease at different levels of biological complexity (molecules, synapses, neural networks and behaviour), ultimately earning a doctorate degree in Health Sciences (2023) from the University of Castilla-La Mancha, Spain.



J. de D. Navarro-López, D. S. del Cerro and L. Jiménez-Díaz contributed equally to this work and they share last authorship.

Abstract Carnitine palmitoyltransferase 1c (CPT1C) is a neuron-specific protein widely distributed throughout the CNS and highly expressed in discrete brain areas including the hypothalamus, hippocampus, amygdala and different motor regions. Its deficiency has recently been shown to disrupt dendritic spine maturation and AMPA receptor synthesis and trafficking in the hippocampus, but its contribution to synaptic plasticity and cognitive learning and memory processes remains mostly unknown. Here, we aimed to explore the molecular, synaptic, neural network and behavioural role of CPT1C in cognition-related functions by using *CPT1C* knockout (KO) mice. *CPT1C*-deficient mice showed extensive learning and memory deficits. The *CPT1C* KO animals exhibited impaired motor and instrumental learning that seemed to be related, in part, to locomotor deficits and muscle weakness but not to mood alterations. In addition, *CPT1C* KO mice showed detrimental hippocampus-dependent spatial and habituation memory, most probably attributable to inefficient dendritic spine maturation, impairments in long-term plasticity at the CA3–CA1 synapse and aberrant cortical oscillatory activity. In conclusion, our results reveal that CPT1C is not only crucial for motor function, coordination and energy homeostasis, but also has a crucial role in the maintenance of learning and memory cognitive functions.

(Received 13 December 2022; accepted after revision 26 May 2023; first published online 12 June 2023)

Corresponding authors J. de D. Navarro-López: D. Soto and L. Jiménez-Díaz: NeuroPhysiology and Behaviour Laboratory, Faculty of Medicine of Ciudad Real, Universidad Castilla-La Mancha, 13071 Ciudad Real, Spain. Email: juan.navarro@uclm.es, davidsoto@ub.edu, lydia.jimenez@uclm.es

Abstract figure legend CPT1C regulates the trafficking of AMPA receptors containing the GluA1 subunit to the membrane surface and the maturation of dendritic spines in the hippocampus. The absence of CPT1C compromises hippocampal synaptic plasticity and cortical oscillatory processes, causes motor and energy dysfunction and induces cognitive deficits affecting associative and non-associative forms of learning and memory.

Key points

- CPT1C, a neuron-specific interactor protein involved in AMPA receptor synthesis and trafficking, was found to be highly expressed in the hippocampus, amygdala and various motor regions.
- CPT1C-deficient animals exhibited energy deficits and impaired locomotion, but no mood changes were found.
- CPT1C deficiency disrupts hippocampal dendritic spine maturation and long-term synaptic plasticity and reduces cortical γ oscillations.
- CPT1C was found to be crucial for motor, associative and non-associative learning and memory.

Introduction

Among the different forms of plasticity, long-term potentiation (LTP) is widely accepted as a cellular correlate for learning and memory. At excitatory synapses, LTP induction and maintenance rely on both structural changes of dendritic spines and the incorporation of AMPA receptors (AMPA receptors) to postsynaptic sites (Bliss et al., 2018; Herring & Nicoll, 2016). These glutamatergic ionotropic receptors are formed by four different subunits (GluA1–GluA4) that can form homo- or heterotetramers with specific properties depending on their subunit composition (Greger et al., 2017). GluA1/GluA2 receptors are essentially added to synapses during synaptic plasticity events, whereas GluA2/GluA3 heteromers continuously replace receptors that are already present at the cell

surface (Shi et al., 2001). The specific behaviour of the different tetrameric receptors is also influenced by a diverse array of proteins that interact with the glutamate-binding pore-forming subunits. These proteins can be auxiliary proteins that are in contact with the receptor at their synaptic targeting site and affect a vast range of AMPAR properties. Examples of such proteins include transmembrane AMPAR regulatory proteins (TARPs), cornichon homologs (CNIHs), or germ cell-specific gene 1-like protein (GSG1L) (Kamalova & Nakagawa, 2021). Additionally, there are proteins that interact with the receptor only transiently during their biogenesis or surface trafficking, such as ferric chelate reductase 1-like (FRRS1L), suppressor of actin 1 (SAC1), Carnitine palmitoyltransferase 1C (CPT1C), or alpha/beta-Hydrolase domain containing 6 (ABHD6)

(Brecht et al., 2017; Schwenk et al., 2019). The important roles of these transiently interacting proteins in AMPAR function are starting to be unraveled.

Recently, one of these transiently interacting proteins, CPT1C, has been identified as a short-lived interactor with AMPARs involved in their synthesis (Fado et al., 2015) and trafficking (Casas et al., 2020; Gratacos-Batlle et al., 2014), but also contributing to dendritic spine maturation (Carrasco et al., 2012). CPT1C is expressed exclusively in neurons located subcellularly at the endoplasmic reticulum (ER) (Sierra et al., 2008), being widely distributed throughout the nervous system and particularly abundant in certain brain areas including the hypothalamus, hippocampus and amygdala (Dai et al., 2007). Some of the CPT1C molecular functions described include the monitoring of malonyl-CoA levels, the modulation of ceramide biosynthesis and the storage of fatty acids in lipid droplets (Casals et al., 2016). Concerning synaptic plasticity, CPT1C-dependent modulation of ceramide content regulates dendritic spine maturation (Carrasco et al., 2012). Additionally, CPT1C interacts with AMPARs at the ER, controlling the amount of GluA1 and GluA2 present at the cell surface (Gratacos-Batlle et al., 2014; Schwenk et al., 2019), and together with FRRS1L, CPT1C interacts with GluA monomeric subunits to induce their dimerization and subsequent tetramerization in the ER (Brecht et al., 2017; Schwenk et al., 2019). In a subsequent stage, tetrameric AMPARs interact with archetypal auxiliary subunits (CNIHs, GSG1L or TARPs) to finally exit the ER (Kamalova & Nakagawa, 2021).

Although CPT1C and FRRS1L participate in the same step of AMPAR biogenesis, patients with mutations in both proteins show completely different symptomatology. FRRS1L mutations cause severe intellectual disability, movement disorders and epilepsy (Brecht et al., 2017), whereas mutations in CPT1C have been related to hereditary spastic paraplegias (HSPs), a group of neurodegenerative disorders characterized by progressive spasticity and weakness of lower limbs. The HSPs are usually classified as complicated or pure, based on the presence or absence of other clinical features, besides the classical motor symptoms. In this regard, two CPT1C variants have been identified to date as the genetic cause of a pure adult-onset autosomal dominant form of the disease, known as hereditary spastic paraplegia 73 (SPG73), which leads to a loss of independent ambulation 10–15 years after the onset of the symptoms in both men and women (Boutry et al., 2019; Hong et al., 2019; Rinaldi et al., 2015). Moreover, two other CPT1C mutations have also been detected in paediatric patients with complicated forms of HSP, one of them causing delay of speech, cortical dysplasia, seizures and hearing impairments (Wang et al., 2023). However, none of these subjects exhibited cognitive alterations. The different outcomes of

FRRS1L and CPT1C mutations in human neurological diseases, with only some common features, suggest a different role for each of the two proteins.

Both FRRS1L and CPT1C knockout (KO) mice exhibit reduced body weight, poor coordination, ataxia and reduced grip strength (Carrasco et al., 2013; Stewart et al., 2019). However, FRRS1L KO mice are hyperactive and showed deficits in LTP and spatial memory (Schwenk et al., 2019; Stewart et al., 2019), whereas CPT1C KO animals are hypoactive (Carrasco et al., 2013; Stewart et al., 2019), with delayed (but not hindered) learning in the Morris water maze (Carrasco et al., 2012), although LTP has never been tested. These data lead to the hypothesis of potential CPT1C functions linked to neuronal activity and plasticity processes required for learning and memory that might remain unknown.

Here, we performed a deep morpho/histological, electrophysiological and behavioural study of animals lacking CPT1C to gain a better understanding of its role in synaptic plasticity and upstream consequences on cognition. CPT1C KO mice exhibited learning and memory deficits in associative and non-associative hippocampus-dependent behavioural tasks. They also showed hypoactivity related to motor dysfunction, but not associated with anxiety- or depression-related behaviours, and failed to learn motor tasks. Electrophysiological recordings showed a decrease in γ oscillations at the posterior parietal cortex (PPC) in behaving mice and alterations in LTP in hippocampal *ex vivo* slices. Finally, these behavioural and electrophysiological impairments were correlated with an increased amount of immaturely glycosylated GluA2 in cerebellar, hippocampal and cortical neurons. Thus, our results reveal a crucial role for CPT1C not only in motor function, but also in motor, associative and non-associative learning.

Methods

Ethical approval

Experiments were carried out in accordance with European Union guidelines (2010/63/EU) and Spanish regulations for the use of laboratory animals in chronic experiments (RD 53/2013 on the care of experimental animals: BOE 08/02/2013) and approved by local Ethic Committees of the University of Castilla-La Mancha (PR-2015-01-01 and PR-2018-05-11) and the University of Barcelona (#117.16 and #164.16). All efforts were made to minimize the pain and suffering of animals. All researchers involved in the study were aware of the ethical principles under which *The Journal of Physiology* operates and complied with the animal ethics checklist set out by *The Journal of Physiology*, the International Council for Laboratory Animal Science and the ARRIVE guidelines.

Animals

Experiments detailed in the flowchart (Fig. 1) were performed on 130 mice (1.2–5 months old); 63 *CPTIC* KO (40 males and 23 females; weighing between 19.8 ± 2.5 and 27.6 ± 3.4 g) and 67 wild-type (WT; 47 males and 20 females; weighing between 18.2 ± 3.4 and 25.2 ± 3.0 g) mice on a C57BL/6J background. The C57BL/6J WT and *CPTIC* KO mice (MGI database ID: 5432790) were provided by the laboratory of Dr Núria Casals (Universitat Internacional de Catalunya). *CPTIC* KO mice were developed as described previously (Carrasco et al., 2012) and presented a genomic deletion including exons 12–15 of *CPTIC*. After eight back-crosses with C57BL/6J mice, littermate homozygous *CPTIC* KO and WT mice were crossed separately to obtain a line for each genotype. At 3 weeks of age, WT or KO newborn mice were weaned, separated, and identified by tail tip genotyping.

Genomic DNA was isolated from tail samples with a Maxwell Mouse Tail DNA Purification Kit (Promega, Madison, WI, USA) following the manufacturer's protocol. Subsequently, a PCR with specific primers to detect the presence of WT *CPTIC* or the inserted neomycin cassette in the KO mice was performed. A fragment of ~280 bp was amplified in WT animals with the primers forward (F9) 5'-GAGTCAGCCATGACC CGACTGTTCC-3' (a sequence inside exon 15) and reverse (R9) 5'-CGCTAAAGCCAGACAGAACACA C-3' (a reverse sequence inside intron 15). A fragment of 200 bp was amplified in KO animals with the

primers forward (R1) 5'-CCGGTAGAATTGACCTGCA GGGGC-3' (inside neomycin cassette) and the same reverse primer previously mentioned (R9). The PCR contained 2 μ l of template DNA (isolated from tail samples), 10 μ l PCR master mix 2 \times (K0171, Thermo Fisher Scientific), 3.2 μ l of primer mixture (final concentration: 1 μ M R9, 0.5 μ M F9 and 0.5 μ M R1) and 4.8 μ l of water for a final volume of 20 μ l. PCR amplifications were carried out with a programmable thermal cycler (Eppendorf AG, Hamburg, Germany). The program used was as follows: 94°C for 2 min, followed by 30 cycles of 94°C for 30 s, 65°C for 30 s and 72°C for 1 min, with a final extension at 72°C for 7 min. PCR products were analysed by electrophoresis in 2% agarose gels.

Mice used in the experiments were initially housed in separate cages (five animals per cage). Those animals that underwent surgery were placed in individual cages after the end of the surgical procedure. The mice were kept on a 12 h light–12 h dark cycle with constant ambient temperature ($21 \pm 1^\circ\text{C}$) and humidity ($50 \pm 7\%$). Unless otherwise indicated, food and water were available *ad libitum*. Cages were cleaned weekly. Additionally, environmental enrichment objects for rodents were always provided.

All tests were performed by an experimenter blind to the genotype of the animals. All behavioural tests were performed during the light phase of the light–dark cycle. Animals were assigned to each experimental group in each experiment after assessing that they did not present any signs of pain, suffering or altered behaviour. Five animals were excluded from further experiments because they showed $\geq 25\%$ weight loss. These animals were not replaced, resulting in accordingly lower final numbers of animals for the respective experiments. In addition, we considered successful experimental animals only those that reached all the behavioural criteria specified on each experiment. The number of successful animals used per experimental group is indicated for each experiment.

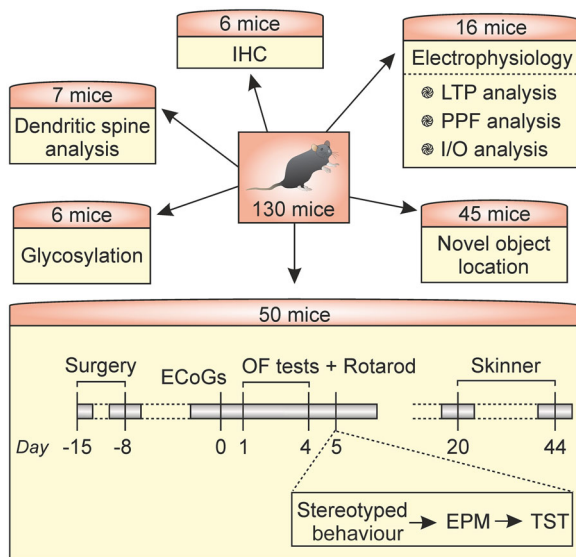


Figure 1. Distribution of animals and time line of experiments

The number of mice used for each specific experiment or group of experiments is indicated. Abbreviations: ECoGs, electrocorticograms; EPM, elevated plus maze; IHC, immunohistochemistry; I/O, input–output curves; LTP, long-term potentiation; OF, open field; PPF, paired-pulse facilitation; TST, tail suspension test. [Colour figure can be viewed at wileyonlinelibrary.com]

Histology and immunohistochemistry

For histological and immunohistochemical studies, animals were deeply anaesthetized with halothane (Fluothane; AstraZeneca, Cambridge, UK) and received buprenorphine intramuscularly as analgesic (0.01 mg/kg; # 062,009, BUPRENODALE; Albet, Barcelona, Spain). Then, mice were transcardially perfused with 0.9% saline (#S9888; Sigma, Poole, UK) followed by 4% paraformaldehyde (#141451; Panreac Applichem, Barcelona, Spain) in PBS (#P4417; Sigma; 0.1 M, pH 7.4). Brains were extracted and cryoprotected with 30% sucrose (#84100; Sigma) in PB. Coronal sections (40 μ m) were cut using a sliding freezing microtome (Microm HM 450; RRID:SCR_015959, Walldorf, Germany) and collected

serially in a solution of glycerol (#G7757; Sigma) and PBS (1:1) for storage at -20°C .

For fluorescence immunohistochemistry, free-floating sections were first treated for 45 min with 10% normal donkey serum (NDS; RRID:AB_2810235, Sigma) in Tris-buffered saline (TBS) containing 0.1% Triton X-100 (TBS-T; #T8532, Sigma) and subsequently incubated overnight at room temperature with polyclonal rabbit anti-CPT1C primary antibody (1:1000; RRID:AB_2782974, Synaptic Systems, Gottingen, Germany) prepared in TBS-T with 0.05% sodium azide (#S/2360/48, Fisher Scientific, Waltham, MA, USA) and 5% NDS. The following day, sections were washed with TBS-T (3×10 min), then incubated for 2 h at room temperature with 1:150 dilutions of FITC-conjugated donkey anti-rabbit (RRID:AB_2315776, Jackson ImmunoResearch, West Grove, PA, USA) in TBS-T. After several washes with TBS (3×10 min), the tissue was incubated in 0.01% DAPI (#sc-3598, Santa Cruz Biotechnology, Santa Cruz, CA, USA) in TBS for 5 min. Finally, sections were rinsed in TBS (3×10 min), mounted on gelatinized glass slides, dehydrated and coverslipped using a fluorescence mounting medium (#S3023, Dako mounting medium, Agilent, Santa Clara, CA, USA). Images were acquired by confocal microscopy at $\times 10$, $\times 20$ or $\times 40$ magnifications using a laser scanning microscope (LSM 800, Carl Zeiss, Jena, Germany).

Deglycosylation assays

Cerebellum, hippocampus and frontal cortex of brains from 1.2-month-old mice were dissected in Hanks' balanced salt solution (HBSS; #24 020-083, Fisher Scientific). Different brain regions were sonicated in PBS with protease inhibitors and phenylmethylsulphonyl fluoride (PMSF; #P7626-1G, Sigma) at 4°C (5 s, four times) and centrifuged at $17,000g$ for 30 min at 4°C . The pellet (membranous insoluble fraction) was resuspended in lysis buffer [1% IGEPAL (#I8896, Sigma), 50 mM Tris-HCl pH 7.5, 150 mM NaCl, 10% glycerol, protease inhibitor cocktail (Roche, Indianapolis, IN, USA) and PMSF], briefly sonicated for 5 s and quantified with a BCA protein assay kit (#K813-2500, Quimigen, Madrid, Spain). For the deglycosylation assay, 20 μg of total protein was mixed with 0.5 M sodium citrate buffer and incubated at 75°C for 15 min to facilitate the access of deglycosylation enzymes to glycidic residues. After cooling the sample, Endoglycosidase-H (EndoH; Roche) was added or not (control sample), and extracts were incubated overnight at 37°C . For N-glycosidase F (PNGaseF)-treated samples, 20 μg of protein was diluted in $1 \times$ Glycoprotein Denaturing Buffer (NEB, Ipswich, MA, USA), incubated at 75°C for 15 min in $1 \times$ GlycoBuffer 2 (NEB), 1% NP-40 and PNGaseF (NEB). These lysates were

incubated for 3 h at 37°C following the manufacturer's instructions.

Samples were separated in 8% SDS-PAGE gels and transferred using Trans-Blot Turbo transfer system on nitrocellulose membranes (all from BioRad, Hercules, CA, USA). Membranes were blocked in TBS-T containing 3% (w/v) bovine serum albumin. The primary antibodies used to detect different proteins were rabbit anti-GluA2 (1:500; RRID:AB_2247874; Merck, Darmstadt, Germany) and mouse anti- β -actin (1:5000; RRID:AB_476743; Merck). Peroxidase-conjugated goat anti-mouse (1:10,000; RRID:AB_10015289; Jackson ImmunoResearch, Ely, UK) or goat anti-rabbit (1:5000; RRID:AB_2313567; Jackson ImmunoResearch, Ely, UK) secondary antibodies, diluted in blocking solution, were detected by using WesternBright ECL (Advansta, San Jose, CA, USA), with the signal detected in the Chemidoc system (BioRad).

Quantification of bands was performed with ImageLab software (BioRad). The percentage of glycosylated and deglycosylated forms of each gel lane was calculated from the total amount of the receptor in the same lane (see Stewart et al., 2019; Tucholski et al., 2014). Untreated samples run in the same gel enabled the determination of the molecular weight of the mature form of the receptor (fully glycosylated) and the quantification of the GluA2/actin ratio as a measurement of total GluA2 protein levels. Likewise, PNGaseF-treated lanes were also run to assess the electrophoretic mobility shift of the totally deglycosylated receptors.

Golgi staining protocol and dendritic spine analysis

Mice ~ 2.4 – 2.6 months old were deeply anaesthetized with sodium pentobarbital (Sigma). Brains were removed, cut into two halves and the left hemispheres prepared for Golgi-Cox impregnation (FD rapid GolgiStain kit; FD Neurotechnologies, Columbia, MD, USA) following the manufacturer's instructions. They were then cut in $150\text{-}\mu\text{m}$ -thick coronal sections using a vibratome. Forty-eight hours later, sections were stained following the same manufacturer's protocol and mounted with DPX mountant for histology (Sigma). Sections of low quality after Golgi staining were discarded. One or two sections per animal were used for quantification of dendritic spines. Dendritic spines of CA1 neurons were visualized in a Zeiss AX10 imager with a $\times 63$ immersion oil objective. Z-stacks were taken every 0.5 – $2\ \mu\text{m}$. Stacks were analysed with Fiji software and counted manually following a standardized protocol (Risher et al., 2014). Immature spines were considered to be those with filopodia ($>2\ \mu\text{m}$ in length) present (Risher et al., 2014). Spines with a head (long thin, thin, stubby, mushroom and branched) were considered mature.

Preparation of hippocampal slices for *ex vivo* electrophysiology

Hippocampal slices were prepared as described previously (Sanchez-Rodriguez et al., 2020). Briefly, animals were deeply anaesthetized with halothane (Fluothane; AstraZeneca), as suggested by the Ethical Committee, because of its high efficacy and rapid action. They were perfused intracardially with 1 ml of oxygenated (95% O₂ + 5% CO₂) ice-cold (4–6°C) artificial cerebrospinal fluid (aCSF), modified with sucrose (234 mM, #84100; Sigma) replacing the NaCl (118 mM, #S9888; Sigma) to minimize damage, and decapitated. The brain was excised and rapidly immersed in oxygenated ice-cold modified aCSF. Horizontal brain slices (300 μm thick) were obtained with a vibratome (7000smz-2; Campden Instruments; Loughborough, UK). Slices were incubated in oxygenated normal aCSF [containing in mmol/L: 118 NaCl, 3 KCl (#P3911; Sigma), 1.5 CaCl₂ (#499609; Sigma), 1 MgCl₂ (#208337; Sigma), 25 NaHCO₃ (#S6014; Sigma), 30 glucose (#G8270; Sigma) and 1 NaH₂PO₄ (#S8282; Sigma), pH 7.35] for 1 h at 30°C, then for ≥1 h at room temperature (22°C) before the recordings.

For electrophysiological recordings, a single hippocampal slice (three or four per animal; *n* = 14 mice) was transferred to an interface recording chamber (BSC-HT and BSC-BU; Harvard Apparatus) and perfused continuously with aCSF. In order to relate neuronal activity and synaptic plasticity in the dorsal hippocampus to learning and memory processes in which this brain region is predominantly involved (mainly cognitive processes related to contextual memory, spatial navigation and object recognition memory), only slices containing the dorsal hippocampus were used.

Extracellular field potentials from CA1 pyramidal neurons were recorded using a borosilicate glass micropipette (1–3 MΩ; RRID:SCR_008593; World Precision Instruments, Sarasota, FL, USA) filled with aCSF, positioned on the slice surface in the stratum radiatum of the CA1 region of the hippocampus and connected to the headstage of an extracellular recording amplifier (NeuroLog System; Digitimer, Welwyn Garden City, UK). Given that synaptic responses were not contaminated by population spikes, the amplitude (i.e. the peak-to-peak value in millivolts during the rise-time period) of successively evoked field excitatory post-synaptic potentials (fEPSPs) was computed and stored for later analysis. For EPSPs, electrical stimuli were applied at 0.2 Hz on the Schaffer collateral pathway through a tungsten concentric bipolar stimulating electrode (TM33CCINS-B; World Precision Instruments) using a programmable stimulator (MASTER-9; A.M.P.I., Jerusalem, Israel). The stimuli presented consisted of 60 μs, biphasic, square-wave pulses presented alone, paired or in trains.

For the construction of the input–output (I/O) curves, paired stimuli with intensities ranging from 0.02 to 0.4 mA were applied at an interstimulus interval of 40 ms. For the paired-pulse facilitation (PPF) protocol, a wide range of interstimulus intervals (10, 20, 40, 100, 200 and 500 ms) was tested, and the stimulus intensity was set well below the threshold for evoking a population spike, ~35% of the intensity necessary for evoking a maximal fEPSP response. For LTP experiments, the synaptic responses were evoked by single pulses applied on the Schaffer collateral pathway, and the intensity was adjusted to the strength necessary for evoking ~40% of a maximal fEPSP. For induction of LTP, the stimulus intensity was also set at ~40% of its asymptotic value, and animals were presented with a high-frequency stimulation (HFS) session (Djebbari et al., 2021) or, alternatively, a θ burst stimulation (TBS) session (Radosevic et al., 2022). The HFS protocol consisted of 100 Hz trains of 1 s duration repeated five times with a 30 s inter-train interval, and the TBS protocol consisted of 10 θ bursts of four pulses of 100 Hz with an inter-stimulus interval of 200 ms repeated seven times with 0.03 Hz. Baseline values for the amplitude of fEPSPs evoked at the CA3–CA1 synapse were collected ≥10 min induction of LTP. After LTP induction, fEPSPs were recorded during ≥60 min.

Surgery and *in vivo* electrophysiological recordings in freely moving mice

Mice were anaesthetized with 4–1.5% isoflurane (induction and maintenance, respectively; #13400264, ISOFLO, Proyma SL, Ciudad Real, Spain) delivered using a calibrated R580S vaporizer (RWD Life Science, Dover, DE, USA; flow rate: 0.5 L/min oxygen) and received buprenorphine intramuscularly as analgesic (0.01 mg/kg; #062009, BUPRENODALE; Albet, Barcelona, Spain) before and after the surgery. Two subdural recording electrodes were implanted over the surface of the posterior parietal cortex of both hemispheres (1.2 mm lateral and 1.8 mm posterior to bregma; Paxinos & Franklin, 2001) to acquire electrocorticographic (ECoG) recordings. These electrodes were made of 50 μm Teflon-coated tungsten wire (Advent Research Materials, Eynsham, UK). A third wire was affixed to the skull as an earth. The two electrodes and the earth were connected to a four-pin socket, and the socket was fixed to the skull with the help of a small screw and dental cement. Immediately after surgery, the animals were placed under a dim red-light warming lamp, and a healing cream (Blastoestimulina; Almirall, Barcelona, Spain) was applied to accelerate recovery and decrease animal suffering. Mice were allowed a week for recovery before the experimental sessions. Handling was performed routinely to minimize mouse stress during experimental manipulation.

In vivo recordings were acquired from alert, behaving mice with EX4-400 Quad differential amplifiers (Dagan, Minneapolis, MN, USA). The ECoGs were recorded from the cortical surface of the behaving animals placed in a plywood box (35 cm × 25 cm × 20 cm) and in the absence of any electrical stimulation.

Behavioural experiments

For habituation to the testing room, mice were weighed in the room and handled under dim light on three consecutive days, for 2 min/day before behavioural testing. The temperature ($21 \pm 1^\circ\text{C}$) and humidity ($50 \pm 7\%$) of the testing room were kept constant.

Open field habituation test. Measurement of exploratory activity in an open field (OF) arena enables the assessment of locomotor activity and anxiety-like behaviour in rodents (Bolivar et al., 2000). However, repeated exposure to the same OF arena is also used to measure habituation (Djebari et al., 2021), an elementary form of non-associative hippocampus-dependent learning. This learning task is termed an OF habituation test and reflects habituation as a decrease in exploratory activity with repeated exposures to the same environment (Leussis & Bolivar, 2006). In this study, habituation memory, locomotor activity and anxiety-like behaviour were evaluated through OF testing using the automated LABORAS system (Laboratory Animal Behaviour, Observation, Registration, and Analysis System; Metris BV, Hoofddorp, The Netherlands), which uses platforms equipped with very sensitive vibration detectors (Djebari et al., 2021). To evaluate habituation learning, mice were exposed to the OF arena in four consecutive sessions (OF1–OF4). Habituation was estimated as the relative decrease in exploratory activity throughout the four sessions (OF1 was considered as a training trial and was compared with the following three retention sessions (OF2–OF4). As an indicator of locomotor activity, the distance travelled in each OF trial was studied. Additionally, anxiety-like behaviour was assessed as the percentage of time spent at the cage periphery (ratio, expressed as percentage, of time spent at the periphery with respect to total test duration) in each OF session. The OF consisted of a LABORAS cage made of 38 cm (length) × 22.5 cm (width) × 4 cm (height) Plexiglas base arena and a 43.5 cm (length) × 27.5 cm (width) × 22.5 cm (height) Plexiglas top. Light conditions were kept at 8–12 lux at the centre of the platform. Animals performed one trial per day on four consecutive days during the morning (09.00–14.00 h). After each trial, the arena was cleaned with 70% EtOH and allowed to dry between animals to remove odours. In each trial, mice were placed in the centre of the OF arena and allowed to explore freely for

15 min. Animal movements were recorded automatically for the 15 min period using the LABORAS system. All data were digitized and analysed using Metris software (Metris BV, Hoofddorp, The Netherlands). For analysis of anxiety-like behaviour, the periphery of the cage was defined as the area between the sidewalls and a virtual line traced 5.4 cm from them throughout the entire perimeter.

Novel object location test. The novel object location (NOL) test, typically used to evaluate hippocampus-dependent spatial learning, was performed in a square box (35 cm × 25 cm × 20 cm) with plywood walls located in a room with dim light. Visual cues were provided within the box and on the walls of the room. Initially, animals were habituated to the test box for 45 min in the absence of any object. Twenty-four hours later, mice underwent the training session, being exposed for 10 min to two identical objects. For the test session, one of the objects was moved to a new location (O1) while the other object remained in the same location (O2). During the test session, conducted 3 h after training, mice were placed in the test box for 9 min. Animals were always placed in the centre of the arena, facing the same direction. The box and objects were cleaned with 70% ethanol between sessions. The exploration time of each object was counted for both training and test sessions. Object exploration was defined as sniffing, touching the object with the nose or pointing the nose towards the object from a distance shorter than ~1 cm. The discrimination index (DI), defined as the difference in exploration time between O1 and O2 divided by the total time spent exploring both objects [$DI = (t_{\text{new}} - t_{\text{familiar}}) / (t_{\text{new}} + t_{\text{familiar}}) \times 100$], was calculated. A value of $DI > 0$ indicates positive discrimination towards the object placed in the new location.

Operant conditioning. To evaluate non-contextual associative memory, an instrumental learning protocol took place in a Skinner box (20.5 cm × 19.5 cm × 22.5 cm; Lafayette Instrument Company, Lafayette, IN, USA) located inside a sound-attenuating chamber (46 cm × 71.5 cm × 43 cm; Campden Instruments, Loughborough, UK). The box was provided with a house light, two levers on the opposite wall with two dim light bulbs above them, a feeder module between the levers and one dispenser of 10% condensed milk coupled to a pump to deliver the liquid into the feeder module after lever pressing (Djebari et al., 2021). Three days before the start and during the experiments, mice were food deprived until reaching 90% of their weight during *ad libitum* diet and maintained at that weight until the end of the operant conditioning experiments. The experimental design was constituted by two different phases: training and light–dark test (L/D test). The training phase consisted of 12 trials performed during 12 consecutive days. In

each trial, the box was constantly illuminated, and mice received condensed milk after each lever press. The total number of lever presses was counted. Mice were allowed to continue with the trial until they spent 20 min in the Skinner box or, alternatively, until they pressed the lever 20 times. Once the animals reached the criterion, which consisted of pressing the lever 20 times per trial for two consecutive days, 20 lever presses were assumed for the remaining trials of the training phase, and they started with the L/D test the following day. The percentage of animals that reached the criterion on each training phase trial was calculated. Animals that did not reach the criterion during the 12 training phase trials were discarded for the L/D test.

For the L/D test, mice underwent 12 trials performed for 12 consecutive days. Light and dark periods of 20 s were alternated until the end of each trial. Under illumination, mice received condensed milk when the lever was pressed, and it was considered as a successful event. In dark conditions, each lever press, considered as a failure, extended the duration of darkness for an extra 10 s, and the animals did not receive any reward. Each trial finished when the animals pressed the lever 20 times in light conditions or, alternatively, after 20 min. The L/D ratio, defined as the difference between successful and failure events divided by the total number of events [$L/D \text{ ratio} = (\text{successes} - \text{failures}) / (\text{successes} + \text{failures})$], was calculated for each trial. In addition, the learning rate was also measured: $\text{learning rate} = [(\text{mean L/D ratio for trials 4 and 5}) - (\text{mean L/D ratio for trials 11 and 12})] / [\text{number of intertrial intervals (which was eight in this study)}]$.

Accelerated rotarod task. A commercially available Plexiglas rotarod apparatus (LE 8500, Panlab SLU, Barcelona, Spain) with automatic timers and falling sensors was used to assess coordination and motor learning. Mice were placed in a 30-mm-diameter black-striated rod. The experimental design consisted of an habituation session performed on the first day (day 1), followed by four test sessions carried out for four consecutive days (days 1–4) during the morning. Each test session was, in turn, constituted by six consecutive trials. In each test session, the animal was placed back on the drum immediately after falling. On the first day, immediately before the test session, the animals were habituated on the drum at a constant speed of 6 r.p.m. for 1 min. For each trial of the test sessions, rotation speed was increased from 4 to 40 r.p.m. in 2 min (cut-off time). The latency to fall off the rod (in seconds) was recorded automatically by the rotarod software. Additionally, the learning rate in each session was calculated as follows: $\text{learning rate} = [(\text{mean latency to fall in trials 5 and 6}) - (\text{mean latency to fall in trials 1 and 2})] / [\text{number of intertrial intervals (which was five in this study)}]$.

Assessment of locomotor activity and stress-related behaviour. To explore the effects of the genotype on locomotor activity and stress-related behaviours, several predefined behavioural categories (grooming, rearing and locomotion) were assessed using the automated LABORAS system. For stereotyped behaviour assessment by LABORAS, each specific behavioural activity is identified based on its characteristic patterns of mechanical vibration, which are recorded continuously (Djebari et al., 2021). Mice were introduced for 15 min (a single trial) into a rectangular empty chamber [23.5 cm (length) \times 17.5 cm (width) \times 4 cm (height Plexiglas base arena, with a 26.5 cm (length) \times 21 cm (width) \times 10 cm (height) top and a cage lid] placed over the LABORAS platforms, and the time spent grooming, rearing and moving was recorded automatically. Light conditions were kept at 8–12 lux at the centre of the platform. Grooming behaviour was used as a measurement of stress-related behaviour (Kalueff & Tuohimaa, 2005). Locomotion and rearing behaviours were used as measurements of locomotor activity. The arena was cleaned with 70% EtOH and allowed to dry between animals to remove odours. All data were digitized and analysed using Metris software.

Elevated plus maze. The elevated plus maze test is a technique that is frequently used to examine anxiety-like behaviour in rodents on the basis of an approach–avoidance conflict. Additionally, locomotor activity can also be estimated. In the present work, both anxiety-like behaviour and locomotion were studied with the elevated plus maze. The maze (LE 842, Panlab SLU) consisted of a cross-shaped methacrylate platform with two open arms without walls and two arms enclosed by 15-cm-high walls, mounted at 90° to one another. Each arm was 65 cm (length) \times 6 cm (width), and the four arms were separated by a central square of 6.3 cm \times 6.3 cm. The structure was elevated 40 cm from the floor. Animals performed a single trial of 5 min. Sessions were recorded using a video camera placed above the arena and scored automatically with Smart video tracking software (Panlab SLU). Mice were introduced into the centre of the platform, facing an open arm at the start of a trial. The total number of entries into the four arms (total arm entries) and number of entries into the closed arm (closed arm entries) were counted as a measure of locomotor activity. To assess anxiety-like behaviour, the percentage of entries into the open arms (open arm entries) and the percentage of time spent in the open arms (ratio, expressed as a percentage, of time spent in the open arms with respect to total test duration) were analysed.

Tail suspension test. The tail suspension test allows the evaluation of energy expenditure, power of movements

and immobility in the same session, thus providing information about muscle strength and energy levels in addition to depression-like assessment (Cryan et al., 2005). In the present work, a tail suspension test automated device (BIO-TST5, BioSeb, Chaville, France) was used. Mice were suspended by the tail with tape (<1 mm from the tip of the tail) to a hook 20 cm in height from the ground. Animals performed a single trial for 6 min. The time of immobility was counted as a measure of behavioural despair, which reflects a condition similar to human depression. Energy expenditure was measured as the total energy spent by the animal during the trial. The power of the movements was calculated from the total energy and discriminates weak and long-lasting from brief and intense movements.

Data collection and analysis

In vivo and *ex vivo* recordings were stored on a computer through an analog-to-digital converter (CED 1401 plus; CED, Cambridge, UK). Electrocardiograms were recorded for 5 min, from which ≤ 3 min of recording, free of unwanted artefacts, was selected for spectral analysis. We selected the following frequency bands: δ (1–4 Hz), θ (4–12 Hz), β (12–30 Hz) and γ (30–100 Hz), based on previous studies (Sanchez-Rodriguez et al., 2017). The power spectrum of the cortical activity was computed with Spike2 software, using the fast Fourier transform with a Hanning window.

Ex vivo recordings were analysed with the program Signal 7 (RRID:SCR_017081). For electrophysiological *ex vivo* data, n represents the number of averaged slices. Evoked synaptic potentials were averaged before I/O, PPF (≥ 5) and LTP (≥ 15) quantitative analyses. In I/O curves, error bars have been omitted to facilitate interpretation of the data.

Statistical analyses of collected data were performed using SPSS v.20 software (SPSS, Chicago, IL, USA). Normal distribution of the data was checked with the Kolmogorov–Smirnov test, and homogeneity of variances was tested with Levene's test. When the distribution of the variables was normal, acquired data were analysed with Student's two-tailed t test or two-way repeated-measures ANOVA, with time (session) and genotype as within-subject and between-subject factors, respectively (except in I/O experiments, in which intensity was the repeated measure). For two-way repeated-measures ANOVA, the Greenhouse–Geisser correction was used and indicated in the text when sphericity was not assumed. The data were grouped according to the genotype to perform intragroup and intergroup comparisons. Non-parametric variables were analysed by using the Mann–Whitney U test. Statistical significance was set at $P < 0.05$. Computed results were

processed for graphical purposes using the software SigmaPlot 12.3 (RRID:SCR_003210). Final figures were prepared using the software CorelDRAW v.18 Graphics Suite (RRID:SCR_014235). Unless otherwise indicated, data are represented as the mean \pm SD.

Results

CPT1C is highly expressed in the hippocampus, amygdala and cerebellum

Given that CPT1C has been shown to be expressed almost exclusively in neurons, we began our study with an immunohistochemical analysis of the CPT1C expression pattern in different areas of the mouse brain. Our immunohistochemical results showed that CPT1C was highly expressed in the hippocampus (Fig. 2A and D), amygdala (Fig. 2G and K) and cerebellum (Fig. 2O and Q). In the hippocampus, CPT1C was predominantly detected in the stratum pyramidale (Fig. 2A), with strong immunoreactivity in pyramidal cell bodies and dendrites of the CA3 and CA1 areas (Fig. 2A–F), crucial regions for spatial learning and memory processes. CPT1C expression was also found to be enriched in brain regions related to emotions (basolateral and central nuclei of the amygdala and the endopiriform nucleus were highly stained; Fig. 2G–J and K–N) and in areas linked to motor function and coordination (cerebellum, striatum and motor cortex; Fig. 2O–T).

CPT1C contributes to GluA1/GluA2 AMPA receptor trafficking

Given that CPT1C controls AMPAR availability by modulating GluA1 translational synthesis and GluA1-containing AMPAR translocation to the post-synaptic membrane (Fado et al., 2015; Gratacos-Batlle et al., 2014), we decided to examine AMPAR trafficking in CPT1C-deficient mice. Recent studies indicate that CPT1C facilitates GluA1-containing AMPAR export from the ER by mediating GluA1 depalmitoylation (Gratacos-Batlle et al., 2018) and Golgi exit through the secretory pathway by the regulation of SAC1 activity (Casas et al., 2020). Here, we assessed the glycosylation state of GluA2 subunits, which serves as a read-out of the number of receptors that traffic properly (Greger et al., 2002; Tomita et al., 2003). Brain extracts from hippocampus, frontal cortex and cerebellum were treated with EndoH and PNGaseF enzymes, which cleave either high-mannose glycans or all N-linked carbohydrates, respectively. Western blot analysis showed that digested GluA2 bands in EndoH-treated samples comigrated with completely deglycosylated subunits obtained by PNGaseF digestion, whereas EndoH-resistant subunits

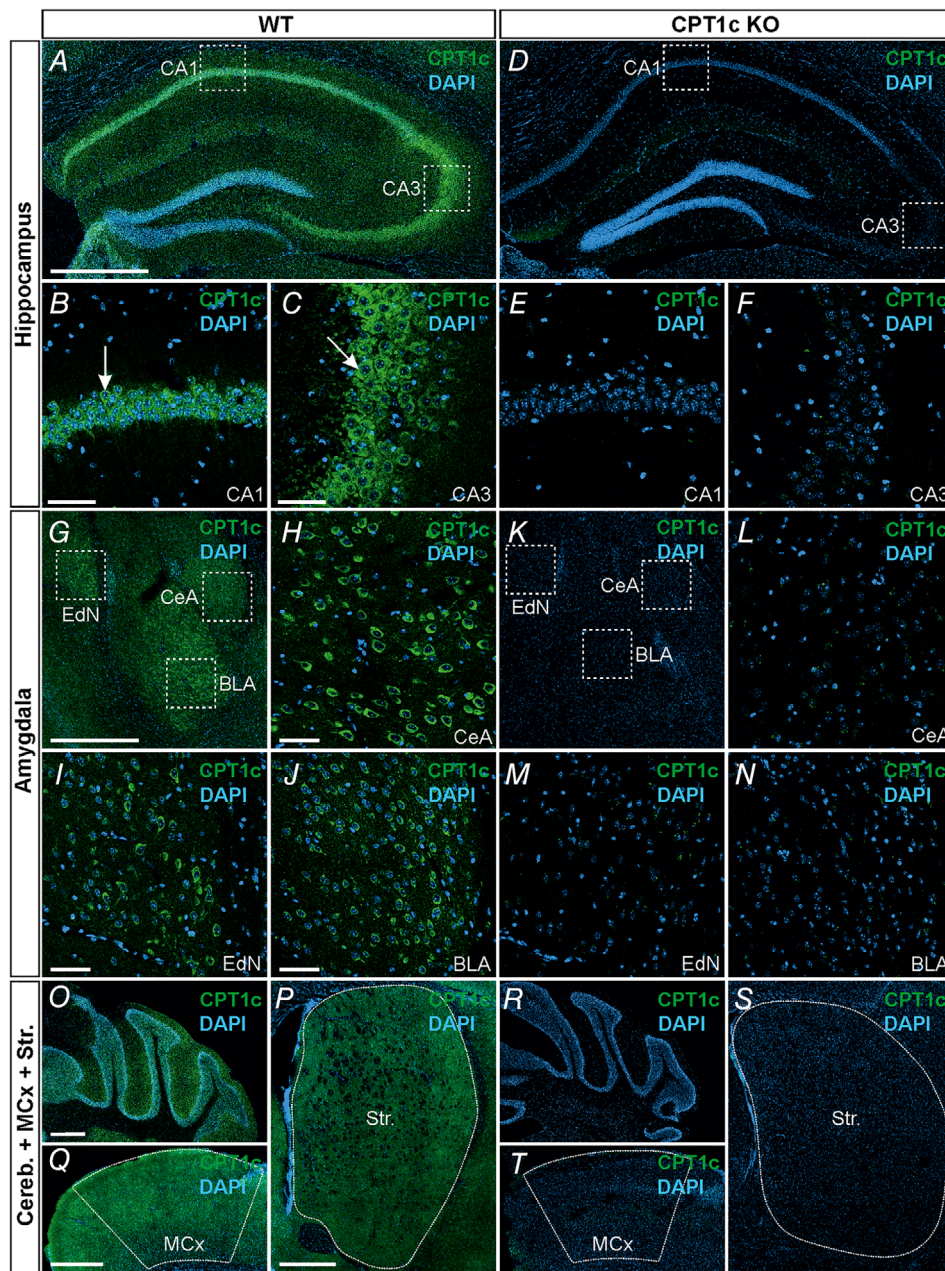


Figure 2. Specific immunohistochemical localization of CPT1C

A–C, G–J, O and P, confocal immunofluorescence images of 40- μm -thick coronal sections immunolabelled with anti-CPT1C antibody (green labelling) and counterstained with DAPI (blue labelling), showing dense CPT1C expression in the hippocampus, cortex and amygdala. A–C, CPT1C immunostaining reveals its high expression in the stratum pyramidale of the hippocampus. CPT1C is densely expressed in pyramidal cell bodies (white arrows) and dendrites of the CA1 (B) and CA3 areas (C). G–J, CPT1C expression is also particularly enriched in the central (H; CeA) and endopiriform nucleus (I; EdN) and in the basolateral nuclei of the amygdala (J; BLA). O–Q, CPT1C immunoreactivity was also found in the cerebellum (O, Cereb.), striatum (P, Str.) and motor cortex (Q, MCx). Squares in A and D indicate the magnified areas displayed in B and C and in E and F, respectively. Squares in G and K indicate the magnified areas shown in H–J and L–N, respectively. Areas within the dashed lines in P and Q correspond to the striatum and motor cortex, respectively. The expression patterns found were specific, because CPT1C immunoreactivity was absent in CPT1C KO mice (D–F, K–N and R–T). Scale bar: 500 μm in A, G and O–Q, also applicable to their CPT1C KO counterparts D, K and R–T; and 50 μm in B, C and H–J, also applicable to their CPT1C KO counterparts E, F and L–N. [Colour figure can be viewed at wileyonlinelibrary.com]

displayed higher molecular weight (Fig. 3A). A higher proportion of EndoH-sensitive GluA2 subunits was found in *CPT1C* KO animals ($n = 3$) compared with WT mice ($n = 3$) in the three examined brain regions [cortex, $n = 3$, $t(2.247) = 4.409$, $P = 0.038$; cerebellum, $n = 3$, $t(4) = 5.029$, $P = 0.007$; and hippocampus, $n = 3$, $t(4) = 6.773$, $P = 0.002$; Fig. 3B], indicating an increased percentage of immaturely glycosylated GluA2 subunits and supporting the notion that GluA1/GluA2 receptor trafficking is hindered. Additionally, given that it had been reported previously that expression of GluA1 and GluA2 subunits was decreased in cultured hippocampal neurons from *CPT1C* KO mice (Fado et al., 2015), we also measured the total protein levels of the GluA2 subunit in the three brain regions studied here and confirmed these findings in the hippocampus. The ratio of GluA2 to actin showed that GluA2 protein levels were reduced in the hippocampus of *CPT1C* KO animals [$t(4) = 3.457$, $P = 0.026$], but not in the cortex [$t(4) = 1.005$, $P = 0.372$] or cerebellum [$t(4) = 1.648$, $P = 0.175$; Fig. 3A and B; complete uncropped western blot membranes including

actin bands are provided as Supporting Information Fig. S1].

Dendritic spine maturation requires CPT1C

To ask whether *CPT1C* deficiency observed in pyramidal dendrites could also affect spine maturation, we calculated the dendritic spine density and performed morphological analysis in Golgi-impregnated hippocampal sections from WT and *CPT1C* KO animals ($n = 3$ and 4 mice, respectively, one or two slices per mouse, 2–10 neurons per slice; Fig. 3C). Although both genotypes exhibited the same dendritic spine density [WT, $n = 3$ animals, 19 neurons, 59 dendrites, number of spines/ $10 \mu\text{m} = 10.45 \pm 2.27$; *CPT1C* KO, $n = 4$ animals, 31 neurons, 63 dendrites, number of spines/ $10 \mu\text{m} = 10.02 \pm 1.20$; $t(5) = 0.327$, $P = 0.757$], neurons from *CPT1C*-deficient mice showed significantly lower levels of mature spines and increased numbers of filopodia [$t(5) = 3.072$, $P = 0.028$; Fig. 3D], indicating the relevance of *CPT1C* for efficient dendritic spine maturation.

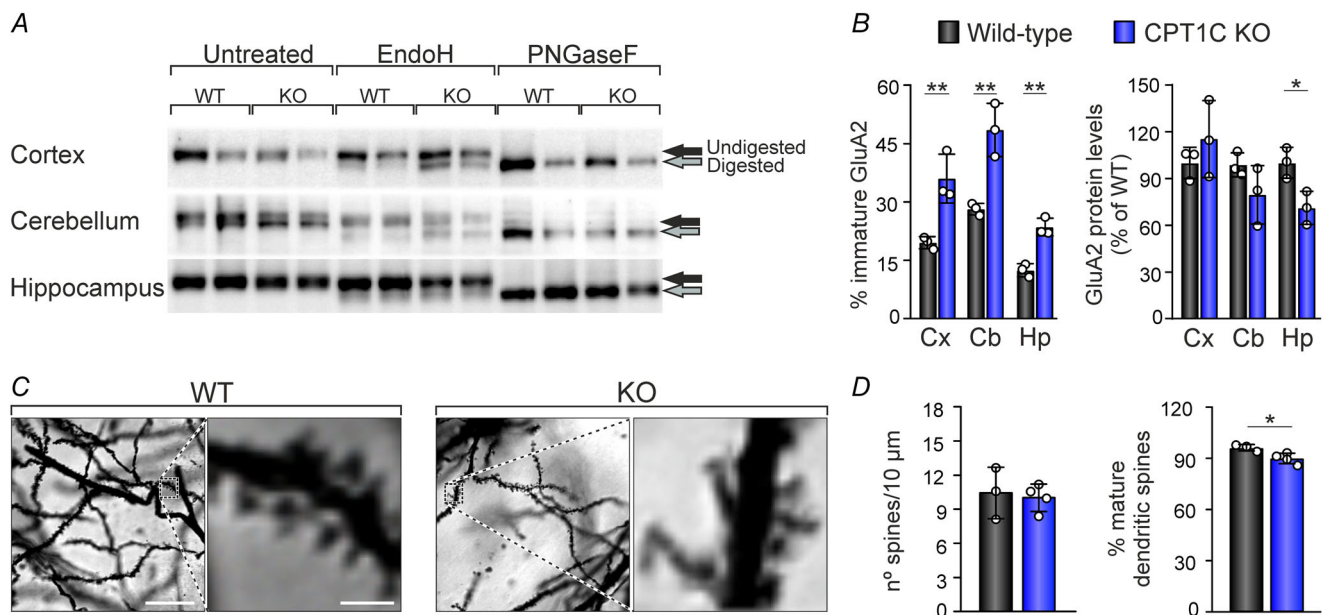


Figure 3. CPT1C deficiency is associated with immature GluA2 glycosylation and impaired dendritic spine maturation

A, the glycosylation state of GluA2 subunits was assessed by western blot analysis in cerebral cortex, cerebellum and hippocampus. The percentage of glycosylated (undigested band) and deglycosylated (digested band) forms in each gel lane was calculated from the total amount of the receptor in the same lane. Untreated samples (for assessment of the molecular weight of the mature form of the receptor) are shown along with samples digested with PNGaseF (to assess the electrophoretic mobility shift of totally deglycosylated receptors) or EndoH enzymes. The GluA2 to actin ratio (for assessment of total GluA2 protein levels) was calculated from untreated samples. B, left bar plot represents the percentage of immaturely glycosylated GluA2 subunits (EndoH-digested band) in the three brain regions. Right bar plot shows the GluA2 to actin ratio as a percentage of wild-type (WT) mean values. C, photomicrographs show representative dendritic spines from WT and *CPT1C* knockout (KO) animals. D, total number of spines per $10 \mu\text{m}$ and percentage of mature dendritic spines for each genotype. Scale bars: left, $20 \mu\text{m}$ and right, $2 \mu\text{m}$ in C; scale bars are applicable to the equivalent images corresponding to *CPT1C* KO mice. Data are represented as the mean \pm SD. * $P < 0.05$, ** $P < 0.01$. Abbreviations: Cx, cortex; Cb, cerebellum; Hp, hippocampus. [Colour figure can be viewed at wileyonlinelibrary.com]

CPT1C deficiency does not modify the excitability of the hippocampal CA3–CA1 synapse *ex vivo*

To determine whether reduced AMPAR trafficking and impaired dendritic spine maturation have a synaptic correlate in *CPT1C* KO mice, neuronal excitability and short- and long-term synaptic plasticity were evaluated at the hippocampal CA3–CA1 synapse. In this regard, the effect of *CPT1C* deficiency on the CA1 hippocampal region was studied by stimulating the Schaffer collateral pathway with different protocols to generate I/O curves and perform PPF analysis.

Electrical stimulation of the Schaffer collaterals evoked a large wave in CA1 pyramidal cells, with a latency of 3.5–4 ms indicating the monosynaptic nature of the responses. Synaptic transmission was measured as changes in the amplitude of the fEPSPs evoked in the CA1 area by paired-pulse stimulation (40 ms interstimulus interval) in hippocampal slices from WT ($n = 4$ mice, 13 slices) and *CPT1C* KO mice ($n = 4$ mice, eight slices). For both experimental groups, the amplitude of fEPSPs evoked by the first pulse increased steadily with the current intensity (range of 0.02–0.4 mA in steps of 0.02 mA; WT, $F_{19,228} = 404.273$, $P < 0.0001$; *CPT1C* KO, $F_{19,133} = 187.023$, $P < 0.0001$; Fig. 4A). The fEPSP amplitudes evoked by the second pulse also increased with current strength (WT, $F_{19,228} = 161.794$, $P < 0.0001$; *CPT1C* KO, $F_{19,133} = 65.314$, $P < 0.0001$) and were larger than those elicited by the first pulse (WT, $F_{2,2,53,3} = 14.435$, $P < 0.0001$; *CPT1C* KO, $F_{19,266} = 7.390$; $P < 0.0001$; Fig. 4B). No significant differences between WT and *CPT1C* KO mice were observed for the I/O curves evoked by first pulse ($F_{1,19} = 0.09876$; $P = 0.7567$) or for the I/O curves elicited by the second pulse ($F_{1,19} = 0.8360$; $P = 0.3720$; Fig. 4A and B). The plot in Fig. 4B, right panel, compares fEPSP amplitudes of the first pulse collected from *CPT1C* KO mice (y -axis) with the corresponding values evoked by the first pulse in WT mice (x -axis) and yields a linear slope close to one ($b = 0.98$), in accordance with an excitability in *CPT1C* KO mice similar to that observed in control animals (Djebari et al., 2021). Together, these results suggest that *CPT1C* deficiency does not significantly alter the excitability of the CA3–CA1 pathway.

Next, we investigated a typical short-term plasticity phenomenon of this synapse known as PPF. Paired-pulse facilitation has been associated with changes in neurotransmitter release and can be used to evaluate pre-synaptic function (Zucker & Regehr, 2002). In addition to the 40 ms interstimulus interval used for the preparation of I/O curves, we tested the enhancement of synaptic transmission evoked by PPF using a wide range of interstimulus intervals (from 10 to 500 ms) at a fixed intensity (~35% of the amount needed to evoke a

maximal fEPSP response). As illustrated in Fig. 4C, both experimental groups (WT, $n = 4$ mice, 13 slices; *CPT1C* KO, $n = 4$ mice, nine slices) exhibited a significant increase of the response to the second pulse at short (20–100 ms) interstimulus intervals (Greenhouse–Geiser correction, $F_{2,7,54,5} = 62.018$, $P < 0.0001$). No significant differences between WT and *CPT1C* KO mice were observed at any of the selected intervals (10, 20, 40, 100, 200 or 500 ms; Greenhouse–Geiser correction, $F_{2,7,54,5} = 0.755$, $P = 0.513$), thus suggesting that *CPT1C* deficiency does not significantly affect short-term hippocampal plasticity and that presynaptic function is not altered.

Ex vivo LTP in dorsal hippocampus needs CPT1C activity

It has been reported previously that basal excitatory synaptic transmission is compromised in *CPT1C* KO animals, in agreement with reduced AMPAR content at synapses and deficient dendritic spine maturation (Fado et al., 2015). Additionally, it is worth mentioning that heteromeric GluA1/GluA2 AMPARs are incorporated into synapses mainly during synaptic plasticity events. Thus, to ascertain whether hippocampal long-term synaptic plasticity is also altered by molecular impairments observed in *CPT1C* KO mice, LTP of the synaptic responses recorded in the CA1 hippocampal region was induced by HFS or, alternatively, TBS of the Schaffer collateral pathway in hippocampal slices from WT (HFS protocol, $n = 6$ mice, 19 slices; TBS protocol, $n = 4$ mice, eight slices) and *CPT1C* KO mice (HFS protocol, $n = 8$ mice, 17 slices; TBS protocol, $n = 8$ mice, 10 slices). Before LTP induction, Schaffer collaterals were stimulated by single pulses for 10 min (0.5 Hz) to obtain a baseline as illustrated in Fig. 4D and F. For LTP induction, slices received an HFS or TBS session (vertical dotted line), and the evolution of the fEPSPs amplitude was analysed for the following 60 min. Both protocols induced LTP in control (HFS protocol, $F_{19,342} = 16.386$, $P < 0.0001$; TBS protocol, $F_{19,133} = 13.616$, $P < 0.0001$) and *CPT1C* KO mice hippocampal slices (HFS protocol, $F_{19,304} = 8.538$, $P < 0.0001$; TBS protocol, $F_{19,171} = 26.439$, $P < 0.0001$). The HFS-induced LTP in WT and *CPT1C* KO mice presented, respectively, a mean potentiation of $146.4 \pm 32.37\%$ and $126.3 \pm 31.9\%$ during, at least, the 60 min. Likewise, the mean potentiation after the TBS protocol was $212.5 \pm 70.3\%$ in control mice and $165.7 \pm 30.3\%$ in their *CPT1C* KO littermates. Interestingly, *CPT1C* KO animals exhibited significantly smaller fEPSP amplitudes 50 min after LTP induction when compared with control mice, regardless of the protocol applied (Fig. 4D and F; HFS protocol, $F_{1,34} = 4.147$, $P = 0.049$; TBS protocol, $F_{1,16} = 4.494$,

$P = 0.049$). The same was found if the last 10 min after the HFS or TBS session were analysed [Fig. 4E and G; HFS protocol, $t(34) = 2.036$, $P = 0.049$; TBS protocol, $t(16) = 2.120$; $P = 0.049$]. Hence, our data indicate that CPT1C deficiency hinders LTP at the CA3–CA1 synapse.

CPT1C KO mice exhibit decreased power spectra of γ oscillatory activity

The PPC is a neocortical brain region interconnected with the hippocampus that is essential for spatial memory and navigation. It has been proposed that the PPC

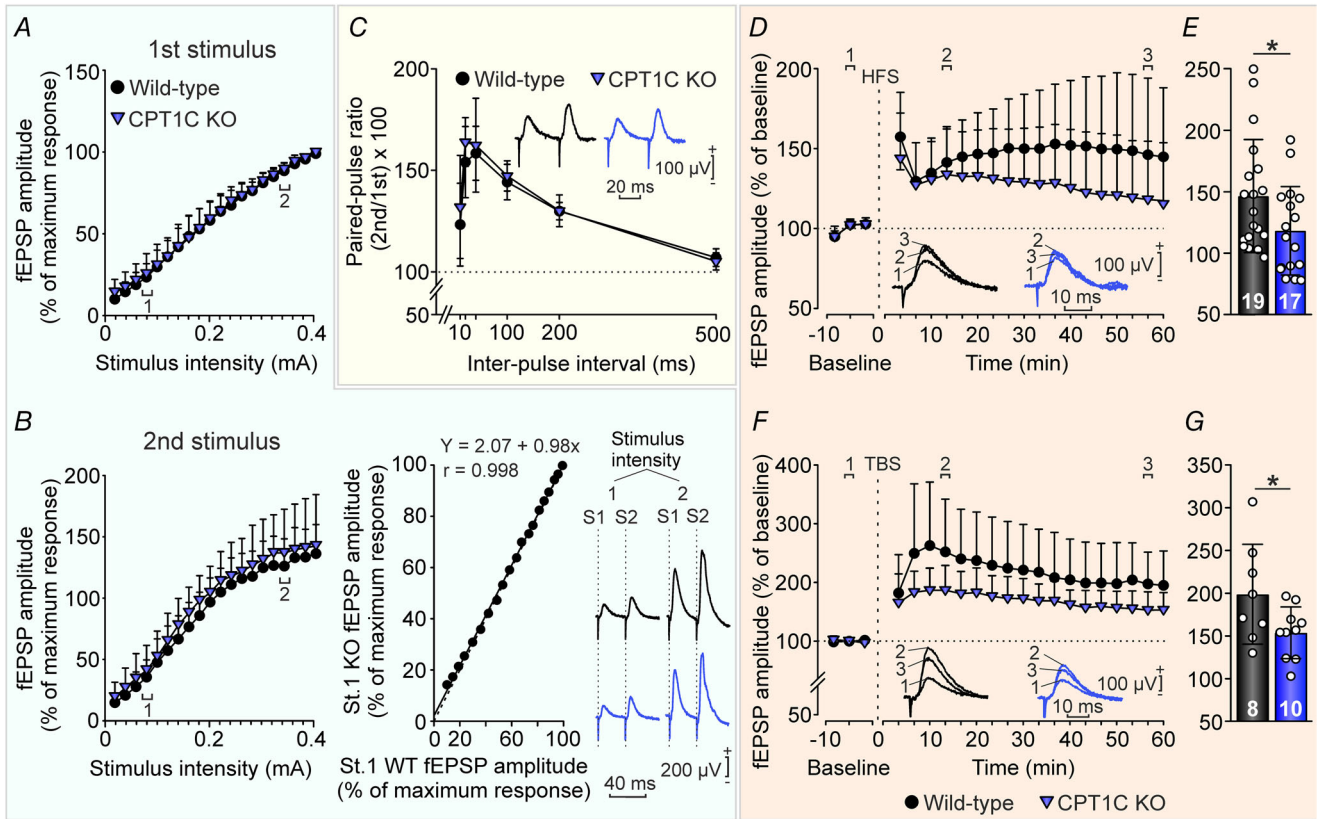


Figure 4. Ex vivo long-term potentiation deficits found at the CA3–CA1 synapse of the hippocampus in CPT1C KO mice

A and left panel of B, relationships between the intensity (in milliamperes) of pairs of stimuli (40 ms interstimulus interval) presented to Schaffer collaterals and the amplitude of the field excitatory postsynaptic potentials (fEPSPs) evoked in the ipsilateral CA1 layer, corresponding to the first (A) and the second (B) pulses in CPT1C knockout (KO) vs. wild-type (WT) mice. Right panel of B, plots and linear fit (black continuous lines) illustrating fEPSP amplitude values evoked by the paired pulses in CPT1C KO vs. WT mice (x-axis, WT; y-axis, CPT1C KO). The dashed line represents a linear fit for control conditions (WT vs. WT). Values were shifted, and the slope of the linear fits was compared with the control to study changes in excitability. Representative averaged fEPSPs (10 responses) recorded in the CA1 area following stimulation at two intensities (intensity 1, 0.08 mA; intensity 2, 0.34 mA; intensities 1 and 2 are indicated in A and left panel of B) are illustrated for each condition (WT, black; CPT1C KO, blue). C, for paired-pulse facilitation (PPF) analysis, averaged fEPSP paired traces for each animal were collected after paired-pulse stimulation at interstimulus intervals of 10–500 ms. The data shown are amplitudes of the second fEPSP expressed as a percentage of the first [(second/first) × 100] for each of the six interstimulus intervals used (paired-pulse ratio). D, evolution of fEPSPs evoked at the CA3–CA1 synapse by stimulation of Schaffer collaterals after an HFS (see vertical dotted line) session. The evolution of LTP was checked by single pulses. Representative averaged fEPSPs recorded in the CA1 area were collected before HFS (1, baseline), 13 min after HFS (2) and ~56 min after HFS (3) for each experimental group. E, bars illustrate the fEPSP amplitude to show the degree of potentiation in the last 10 min after the HFS session. F, evolution of fEPSPs evoked at the CA3–CA1 synapse by stimulation of Schaffer collaterals after a TBS (see vertical dotted line) session. The evolution of LTP was checked by single pulse stimulation. Representative averaged fEPSPs recorded in the CA1 area were collected before TBS (1, baseline), 13 min after TBS (2) and ~56 min after TBS (3). G, bars illustrate fEPSP amplitude to show the potentiation level in the last 10 min after the TBS session. For LTP experiments, the number of slices for each condition is indicated in the bar plots. Data are represented as the mean ± SD. * $P < 0.05$ vs. WT. [Colour figure can be viewed at wileyonlinelibrary.com]

integrates hippocampal information about allocentric representations of the space, transforming them into egocentric reference frames that the animal uses to direct locomotion (Burgess et al., 2002; Whitlock et al., 2008). Likewise, the PPC sends egocentric information to the hippocampus to generate allocentric maps (Bicanski & Burgess, 2018). To assess whether alterations of synaptic transmission and plasticity in *CPT1C* KO mice disrupt hippocampal and parietal network activity, we next examined oscillatory activity recorded from the surface of the PPC in freely moving mice with chronically implanted subdural electrodes (Fig. 5A). Power spectra of frequency intervals corresponding to δ (1–4 Hz), θ (4–12 Hz), β (12–30 Hz) and γ (30–100 Hz) rhythms were analysed in EcoG recordings (Sanchez-Rodriguez et al., 2017).

As shown in Fig. 5B, no differences between WT ($n = 23$) and *CPT1C* KO animals ($n = 14$) were found for the δ , θ and β frequency bands (δ , $U = 149$, $P = 0.707$; θ , $U = 152$, $P = 0.778$; and β , $U = 109$, $P = 0.103$). However, control mice showed greater power spectra than their *CPT1C* KO counterparts for the γ rhythm oscillations ($U = 76.5$, $P = 0.005$). These neural network alterations in KO mice could account for potential memory disruption, because they have been related previously to learning

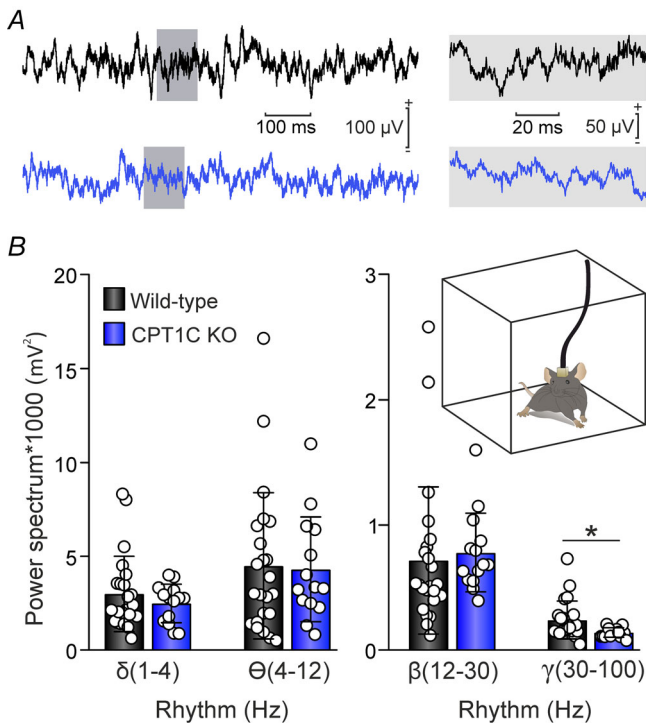


Figure 5. Spectral power distribution of electrocorticogram recordings collected in freely moving mice

A, representative examples of electrocorticogram recordings in wild-type (WT; black) and *CPT1C* knockout (KO) mice (blue) on different time scales. B, bar plots illustrate mean \pm SD power spectra of oscillatory activity recorded at frequency intervals corresponding to δ , θ , β and γ rhythms. * $P < 0.05$ vs. WT. [Colour figure can be viewed at wileyonlinelibrary.com]

and memory deficits together with synaptic plasticity impairments (Frieze et al., 2013), also found in *CPT1C* KO mice in the present work.

CPT1C deficiency impairs motor function and coordination

CPT1C has been shown to play a crucial role in energy homeostasis, motor function and coordination, being impaired progressively with age in *CPT1C* KO mice (Carrasco et al., 2013). Here, before studying its physiological role in learning and memory, we characterized these deficiencies in animals aged 3–4 months.

First, locomotor activity was assessed in an OF arena with the LABORAS system (WT, $n = 25$; *CPT1C* KO, $n = 22$), which tracked the movements of the animals automatically. As shown in Fig. 6A, this revealed that *CPT1C* KO mice not only spent less time moving, but also travelled significantly shorter distances (WT, 15.17 ± 5.18 m; *CPT1C* KO, 7.24 ± 3.18 m; $P < 0.0001$ in all sessions). Likewise, the LABORAS system was used for automated assessment of different stereotyped behavioural activities. As illustrated in Fig. 6B, mice were placed in empty cages to measure the time spent grooming and rearing along with overall locomotion. The *CPT1C* KO animals ($n = 22$) again showed significantly lower locomotor activity [$t(45) = 8.7$, $P < 0.0001$] and rearing [$t(45) = 7.5$, $P < 0.0001$] than WT mice ($n = 25$). On the contrary, grooming behaviour was increased [$t(27\ 647) = -6$, $P < 0.0001$], very probably caused by long time periods of immobility rather than stress (Kalueff & Tuohimaa, 2005). In addition, we examined general locomotor activity using the elevated plus maze. As expected, we found a significantly lower number of entries into the closed arms ($U = 145.5$, $P = 0.006$) and total arms ($U = 173$, $P = 0.029$) of the platform in *CPT1C* KO animals (Fig. 6C), thereby confirming locomotor impairments associated with *CPT1C* deficiency. We wondered whether these motor impairments were manifested as decreased energy expenditure and/or reduced muscle strength. In this regard, the tail suspension test (WT, $n = 25$; *CPT1C* KO, $n = 22$) unveiled low energy levels [$t(30.44) = -4.4$, $P = 0.0001$] and reduced power of the movements ($U = 116$, $P = 0.0006$) in *CPT1C* KO mice (Fig. 6D), indicating that motor dysfunction associated with the absence of *CPT1C* is linked to energy shortage and/or muscle weakness.

CPT1C does not play a role in anxiety- and depression-like behaviour

Given that *CPT1C* is highly expressed in brain areas related to emotions, namely the amygdala and

hippocampus, we next explored the effects of CPT1C deficiency on anxiety and depression by performing several behavioural tasks. Additionally, this approach was aimed to discard potential changes in emotional state that could bias the interpretation of the results obtained in learning and memory tasks or motor function tests. In the OF arena, *CPT1C* KO mice ($n = 22$) spent a greater percentage of time in the cage periphery ($95.9 \pm 3.99\%$) than control animals ($n = 25$; $87.3 \pm 7.83\%$; $P < 0.0001$ in all sessions; Fig. 6E), which might indicate higher anxiety levels. However, no significant differences

were observed in the elevated plus maze (WT, $n = 25$; *CPT1C* KO, $n = 22$; Fig. 6F), either for the percentage of open arm entries [$t(45) = 0.932$, $P = 0.356$] or for the percentage of time spent in open arms ($U = 239$, $P = 0.443$), two parameters linked to anxiety-related behaviours. Together, these findings suggest that the differences found in the OF might be ascribed to the periods of immobility that *CPT1C* KO mice prefer to spend in the periphery, as a consequence of their motor impairments, rather than anxiety-like symptoms. In contrast, when the time of immobility was assayed in the

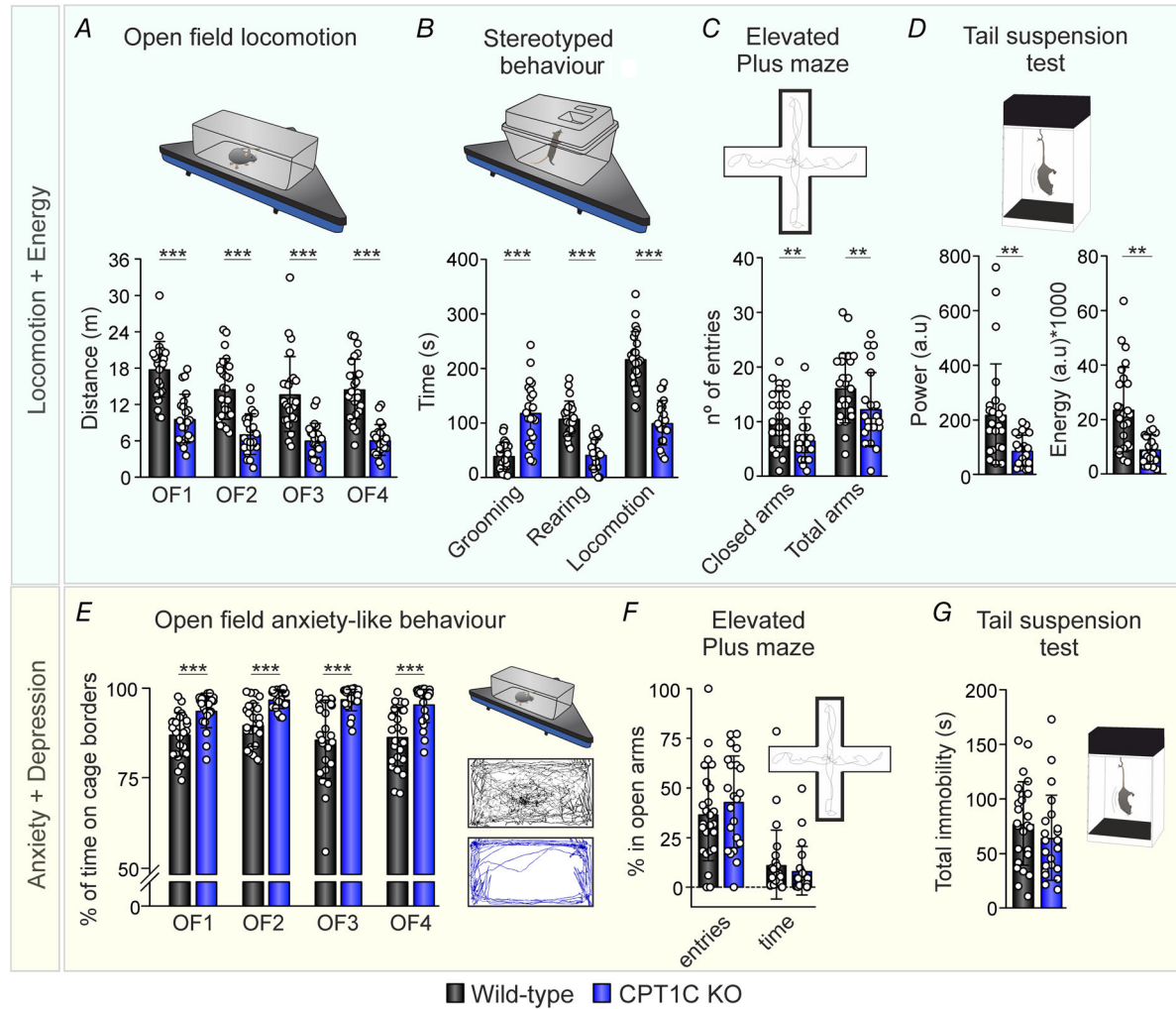


Figure 6. CPT1C deficiency causes reduced energy expenditure and locomotor activity (top) but does not affect mood state (bottom)

A and E, the schematic representation illustrates the open field arena and LABORAS system. Bar plots represent quantification of the distance travelled (A) and percentage of time spent on cage borders (E). Representative tracks in the arena are also displayed (E). B, the schematic representation illustrates the LABORAS system and cage for assessment of spontaneous behaviour. Bar plots display quantification of the time that mice spent grooming, rearing and moving. C and F, the schematic representation illustrates the elevated plus maze with two open and two closed arms. Bar plots display quantification of the number of entries into closed arms and total arms (C) and the percentage of time spent in open arms and percentage of open arm entries (F). D and G, the schematic representation illustrates the tail suspension test. Bar plots show quantification of the energy, power (D) and total time of immobility (G). Abbreviation: OF, open field session. Data are represented as the mean \pm SD. ** $P < 0.01$, *** $P < 0.001$ vs. WT. [Colour figure can be viewed at wileyonlinelibrary.com]

tail suspension test (WT, $n = 25$; *CPT1C* KO, $n = 22$) as an indicator of depression-related behaviour, no differences between groups were found [$t(45) = -1.143$, $P = 0.259$; Fig. 6G]. Thus, our data do not show a clear effect of *CPT1C* deficiency on mood state.

CPT1C deficiency impairs different types of learning

Having established that *CPT1C* deficiency impaired the maturation of dendritic spines and AMPAR trafficking with consequences for synaptic plasticity and network activity, we wondered about the outcomes of these alterations at the cognitive level, given that successful learning and memory encoding is highly sensitive to the network oscillatory activity that arises from neuronal synchronous firing patterns (Palop et al., 2006). In order to assess hippocampal function, mice were challenged to hippocampus-dependent memory tasks, including the OF habituation test and the NOL test. Briefly, the OF habituation test relies upon the tendency of rodents to reduce their exploratory behaviour when repeatedly exposed to the same environment, which is reflected as a progressive decrease in locomotor activity (Leussis & Bolivar, 2006). Here, the mean locomotor activity of WT mice was decreased significantly to $80.7 \pm 25.59\%$ in sessions 2–4 with respect to the training session 1 ($n = 25$, $F_{2,13,51.23} = 4.89$, $P = 0.01$, Greenhouse–Geisser correction) as illustrated in Fig. 7A, whereas the movement of *CPT1C* KO mice was reduced to $73 \pm 33.32\%$ ($n = 22$, $F_{1,61,33.89} = 3.27$, $P = 0.06$, Greenhouse–Geisser correction). These results show that habituation memory across the three retention OF sessions (OF2–OF4) was slightly, though not significantly, preserved in *CPT1C* KO mice.

On the other hand, the NOL test was carried out to measure the ability of the animals to recognize a new spatial distribution of familiar objects, thereby assessing hippocampus-dependent spatial learning. For this purpose, mice were familiarized with two identical objects during the training period. As expected, WT ($n = 25$) and *CPT1C* KO ($n = 19$) animals explored both objects equally during the training phase, yielding a discrimination index close to zero [DI = 0 indicates no discrimination or preference for a particular object; WT, $t(24) = 0.541$, $P = 0.593$; *CPT1C* KO, $t(18) = 0.358$, $P = 0.725$; Fig. 7B]. Three hours later, one of the objects was moved, in order to evaluate short-term spatial memory. The WT mice preferentially explored the object in the new location [$t(24) = 3.948$, $P = 0.0006$], but their *CPT1C* KO counterparts did not [$t(19) = 0.197$, $P = 0.846$; Fig. 7A], indicating short-term memory deficits that might be linked to the absence of *CPT1C* in the hippocampus.

Given that *CPT1C* deficiency has been linked to deficits in motor function and coordination, we also asked whether motor learning ability would be compromised in *CPT1C* KO mice, considering *CPT1C* expression patterns in the cerebellum and motor cortex (Carrasco et al., 2013). In the accelerating rotarod task, mice underwent an increasing rotational speed in each session, and the latency to fall off the rod was measured. The *CPT1C* KO mice ($n = 21$) exhibited shorter latencies to fall than their WT counterparts ($n = 25$) in every session (session 1, $P = 0.0003$; session 2, $P = 0.0001$, sessions 3 and 4, $P < 0.0001$; Fig. 7C, left panel), suggesting locomotor impairments since the beginning of the task. In addition, *CPT1C* KO mice did not show a significant progression (latency in sessions 2–4 = $96.1 \pm 34.53\%$ of session 1; $F_{23,460} = 0.563$, $P = 0.951$) across the four sessions unlike control animals ($n = 25$; latency in sessions 2–4 = $148.2 \pm 67.87\%$ of session 1; $F_{5,34,128.13} = 8.78$, $P < 0.0001$, Greenhouse–Geisser correction; Fig. 7C, middle panel), confirming motor learning deficits. In fact, WT mice exhibited a significant learning rate during both the first and last sessions [session 1, $t(24) = 3.675$, $P = 0.0012$; session 4, $t(24) = 4.672$, $P < 0.0001$], whereas the learning rate of *CPT1C* KO mice was not significant in any of them [session 1, $t(20) = 0.530$, $P = 0.602$; session 4, $t(20) = 0.519$, $P = 0.609$; Fig. 7C, right panel]. Nonetheless, these findings must be interpreted with caution, because the inability of *CPT1C*-deficient mice to exhibit a progression in this task might be attributable to muscle weakness and/or other locomotor impairments rather than a consequence of the alterations in synaptic plasticity in brain areas required for motor learning.

Finally, the involvement of *CPT1C* in non-contextual associative instrumental learning was also assessed in the Skinner box model. In this task, mice first performed a training phase under constant illumination, in which each lever press was reinforced with 10% condensed milk as a reward. The criterion to complete the task consisted of 20 lever presses per session on two successive days. Both experimental groups improved their performance progressively over the sessions (WT, $n = 14$, $F_{2,83,36.89} = 23.86$, $P < 0.0001$, Greenhouse–Geisser correction; KO, $n = 12$, $F_{2,47,27.14} = 6.77$, $P = 0.002$; Fig. 7D, left plot). However, control mice progressed slightly, albeit not significantly ($F_{1,24} = 2.44$, $P = 0.131$), faster than *CPT1C* KO animals, and significant differences between groups arose in the last two sessions (session 11, $U = 48$, $P = 0.023$; session 12, $U = 48$, $P = 0.024$). In addition, a higher percentage of WT mice (85.7%) reached the criterion within the 12 sessions when compared with their *CPT1C* KO littermates (50%; Fig. 7D).

In the second phase, the light–dark test, mice that reached the criterion within the 12 training sessions were subjected to another task with a new level of complexity. Light and darkness were alternated, and

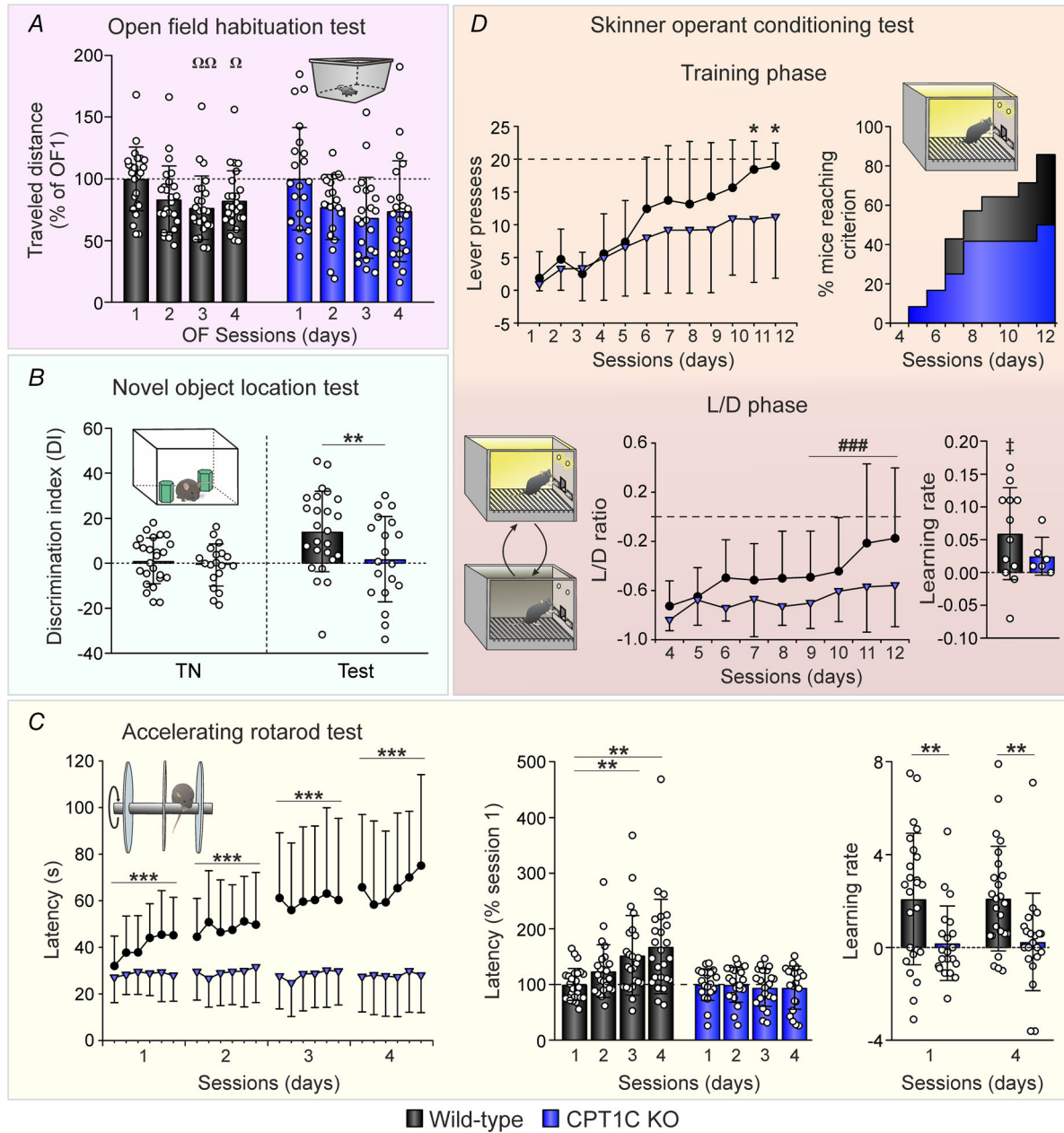


Figure 7. CPT1C KO mice exhibit hippocampus-dependent learning and memory impairments and motor learning deficits

A, open field (OF) habituation test. Habituation memory was evaluated by measuring the distance travelled in four sessions (OF1–OF4) performed on consecutive days. Data are expressed as percentage of session 1 (OF1). B, novel object location test. The discrimination index [DI = $(t_{\text{new}} - t_{\text{familiar}}) / (t_{\text{new}} + t_{\text{familiar}}) \times 100$] is represented for the training (TN) and test sessions. C, left, performance at the accelerated rotarod task was evaluated by measuring the latency to fall in each trial during four consecutive days. Each day, mice were exposed to six trials. The middle bar plot represents mean time to fall on each day expressed as a percentage of session 1 latency. Right, the learning rate (LR) during sessions 1 and 4 was calculated as: $LR = [(mean\ latency\ to\ fall\ in\ trials\ 5\ and\ 6) - (mean\ latency\ to\ fall\ in\ trials\ 1\ and\ 2)] / 5$. D, Skinner operant conditioning test. Animals were challenged in two different phases of increasing difficulty, namely a training phase and an light/dark (L/D) phase. Left plot, the mean number of lever presses during the training phase is represented. For those mice that reached the criterion in a specific session (20 presses per session on two consecutive days) of the training phase, 20 lever presses were assumed for the following sessions. The cumulative percentage of mice that reached the criterion is represented for each session. For the L/D experiment, the L/D ratio [coefficient L/D = $(successes - failures) / (successes + failures)$] of sessions 4–12 was calculated. Learning rate, defined as the difference between the mean L/D ratio of the two last sessions and the mean L/D ratio of the two sessions with the worst performance (sessions 4 and 5), and divided by the

number of intervals between sessions [learning rate = [(mean L/D ratio in sessions 11 and 12 – mean L/D ratio in sessions 4 and 5)/8]], is also represented. Data are represented as the mean \pm SD. $^{\Omega}P < 0.05$, $^{\Omega\Omega}P < 0.01$ intragroup differences vs. OF1; * $P < 0.05$, ** $P < 0.01$, *** $P < 0.001$ vs. WT; ### $P < 0.001$, intragroup differences across sessions; # $P < 0.05$ vs. 0. [Colour figure can be viewed at wileyonlinelibrary.com]

rodents were instructed to press the lever only when the light bulb was switched on. Lever presses in lighted periods were rewarded, whereas each lever press in dark conditions did not provide the reward and delayed the appearance of the following illuminated period (see Methods). Our data showed that WT mice ($n = 12$) improved their performance significantly throughout the sessions (sessions 9–12, $F_{3,33} = 7.57$, $P = 0.0005$), but their *CPT1C* KO counterparts did not ($n = 6$, $F_{3,15} = 1.04$, $P = 0.402$; Fig. 7D, right plot). Indeed, the learning rate (see Methods) was significant only in control mice [WT vs. 0, $t(11) = 3.006$, $P = 0.012$], as shown in Fig. 7D (right bar plot). In summary, these results suggest that *CPT1C* also plays an important role in associative learning.

Discussion

In this work, we reveal a crucial role for *CPT1C* in associative and non-associative learning and memory and in motor function.

CPT1C deficiency impairs overall motor function, coordination and motor learning

An important role of *CPT1C* in motor function, coordination and muscle strength has been reported (Carrasco et al., 2013). Indeed, the striatum, motor cortex and cerebellum are among the brain areas with evident *CPT1C* expression, as we confirmed through immunohistochemical analysis. Locomotor activity impairments, incoordination and muscle weakness have been reported in *CPT1C* KO mice, probably arising from weaning (postnatal day 21) and worsening during early adulthood (Carrasco et al., 2013). Here, our approach focused on adulthood, and our cohort of 12- to 24-week-old *CPT1C* KO animals showed reduced locomotor activity and incoordination in rotarod activity, in addition to decreased locomotion in OF and plus maze arenas. Consistently, rearing activity was decreased as *CPT1C* KO mice experienced longer periods of immobility. On the contrary, grooming, an innate behaviour increased by low-, mild- or high-stress situations (Kalueff & Tuohimaa, 2005), was augmented in *CPT1C* KO mice very probably owing to both their higher immobility and certain stress (either low stress in resting conditions or mild stress in response to a new environment). Additionally, energy expenditure and the power of the movements, a parameter of tail suspension testing that measures weak or intense

movements, were also noticeably impaired, indicating energy deficits and/or muscle weakness.

Interestingly, the motor deficits observed in *CPT1C* KO mice recapitulate some of the symptoms of human *CPT1C* deficiency (Rinaldi et al., 2015), which is associated with HSP, a motor corticospinal neuron axonopathy that causes slowly progressive weakness, spasticity of the muscles of the legs and reduced motility (Blackstone et al., 2011). Impairment of organelle transport along the axon is a common trait of HSP (Boutry et al., 2019), and *CPT1C* has recently been shown to be involved in the regulation of late endosome/lysosome axon transport (Palomo-Guerrero et al., 2019). Therefore, impaired axon transport caused by *CPT1C* deficiency is likely to contribute to motor deficits of *CPT1C* KO mice. However, given that *CPT1C* KO mice show altered energy homeostasis and metabolic inflexibility (Casas et al., 2020; Pozo et al., 2017), we cannot discard the possibility that impaired muscle energy metabolism contributes to their reduced locomotion and motor dysfunction. In hypothalamic neurons, *CPT1C* acts as a sensor of the energy status by binding malonyl-CoA and modulates ceramide synthesis and food intake through its participation in anorexigenic/orexigenic signalling pathways (Wolfgang & Lane, 2011). Together, these altered processes might contribute to the energy deficiencies in *CPT1C* KO mice.

Furthermore, motor deficits have also been associated with *CPT1C*-dependent alterations of ceramide and sphingosine levels in motor brain areas such as the cerebellum, striatum and motor cortex (Carrasco et al., 2012; Carrasco et al., 2013). Indeed, low levels of ceramide and its derivatives lead to neurodegeneration and abnormal dendritic development in Purkinje cells (Furuya et al., 1998; Zhao et al., 2011). Likewise, ceramide plays a protective role in motoneurons against oxidative cytotoxicity (Irie & Hirabayashi, 1999). Thus, motor dysfunction associated with *CPT1C* might arise from the combination of energy shortage affecting skeletal muscles, compromised corticospinal tract integrity and altered lipid metabolism in motor brain areas.

The aforementioned processes should be also taken into account to explain the inability of *CPT1C* KO mice to improve their motor skills in the rotarod task. However, alterations in synaptic plasticity might also contribute significantly to motor learning deficits. *CPT1C* promotes efficient spine maturation by increasing ceramide levels and regulates the efficiency of AMPAR synthesis and trafficking to the cell surface (Carrasco et al., 2012; Casals et al., 2016; Casas et al., 2020; Gratacos-Batlle et al., 2014), affecting synaptic formation,

maturation and maintenance (McKinney, 2010). During motor learning, LTP is induced in primary motor cortex neurons, promoted by structural remodelling and increased GluA1-containing AMPARs in dendritic spines (Kida & Mitsushima, 2018; Padmashri et al., 2013; Roth et al., 2020). Even at parallel fibre–Purkinje cell synapses, LTP is mediated by GluA2 insertion in the postsynaptic membrane, contributing to cerebellar motor learning (Grasselli & Hansel, 2014; Kakegawa & Yuzaki, 2005). In this context, CPT1C regulates GluA1 translational synthesis (Fado et al., 2015) and is abundant in the periphery of native AMPAR complexes (Chen et al., 2014; Schwenk et al., 2012), although they colocalize only at the ER (Gratacos-Batlle et al., 2014). In fact, the expression profile of both GluA1 and GluA2 subunits parallels CPT1C expression in the hippocampus (Fado et al., 2015), although current evidence points to a GluA1 subunit-specific interaction, because CPT1C does not increase surface expression or whole-cell currents in cells expressing homomeric GluA2 receptor (Gratacos-Batlle et al., 2014; Schwenk et al., 2012). Additionally, CPT1C-mediated depalmitoylation of GluA1 and inhibition of SAC1 catalytic activity prevents AMPAR retention at the Golgi apparatus, facilitating its export from the ER to the postsynaptic membrane (Casas et al., 2020; Gratacos-Batlle et al., 2018). In the present study, given that it has been suggested that only maturely glycosylated GluA2 subunits are present at the cell surface (Greger et al., 2002; Sans et al., 2001), we performed an EndoH sensitivity assay that revealed a lower ratio of mature to immature GluA2 subunits in the cortex and cerebellum of *CPT1C* KO mice, suggesting that CPT1C facilitates GluA1/GluA2 heteromeric AMPAR trafficking to the cell surface in motor areas. Therefore, deficits in both CPT1C-dependent AMPAR synthesis and trafficking to the postsynaptic membrane might be hindering LTP in those regions, as occurs with GluA1 hyperpalmitoylation in the hippocampus (Spinelli et al., 2017). However, further studies are needed to determine the brain regions that constitute the origin of the motor dysfunction and motor learning deficits in CPT1C-deficient mice. In this regard, selective deletion of the protein in specific brain areas might provide particularly valuable new insights.

CPT1C does not affect anxiety- and depression-like behaviours

To date, no CPT1C functions related to anxiety, stress or depression have been described, despite its widespread distribution across the brain and its strong presence in the amygdala and the hippocampus, as found here. However, the abundance of ceramide in both regions has been associated with anxiety- and depression-like behaviour, respectively (Gulbins et al., 2013; Zoicas et al., 2020).

The CPT1C deficiency might modify the susceptibility to develop anxiety- or depression-like behaviour through CPT1C-induced modulation of ceramide levels. Although in the OF test *CPT1C* KO animals spent more time in the periphery, which is interpreted as a sign of anxiety-like behaviour, this test has not shown complete validity for general assessment of anxiety and, consequently, might lead to misinterpretation of the data (Prut & Belzung, 2003). In this regard, more time in the periphery might not be attributable to anxiety-like behaviour, but might be caused by reduced locomotor activity and longer periods of immobility that rodents spontaneously prefer to spend near the edges of the OF arena. Indeed, elevated plus maze results showed anxiety levels similar to those of control mice. Moreover, *CPT1C* KO mice did not exhibit significant depression levels in the tail suspension test. Thus, despite CPT1C involvement in ceramide metabolism, our data do not provide evidence to suggest its involvement in mood status, with neither anxiety- nor depression-like behaviour.

Excitability and synaptic plasticity at the CA3–CA1 synapse of CPT1C-deficient mice

Confirming the expression patterns reported by previous studies (Carrasco et al., 2013; Dai et al., 2007), here we found CPT1C to be highly expressed in hippocampal CA3 and CA1 areas, with a particularly strong CPT1C presence in pyramidal cell bodies and dendrites. As expected, based on the described role of CPT1C in modulating AMPAR function, mediated miniature EPSPs driven by AMPARs in cultured hippocampal pyramidal cells lacking CPT1C protein were reduced (Fado et al., 2015), potentially compromising basal synaptic transmission and neural network activity. Conversely, our *ex vivo* results of synaptic transmission showed that neuronal excitability and presynaptic function were preserved at the CA3–CA1 synapse of *CPT1C* KO mice. However, the study of long-term plasticity showed that both HFS and TBS protocols induced LTP in CPT1C-deficient mice with significantly reduced magnitude. This LTP impairment is consistent with dampened AMPAR synthesis and trafficking to the postsynaptic membrane, an indispensable process for LTP induction that probably cannot be compensated by other mechanisms (Herring & Nicoll, 2016).

CPT1C deficiency causes aberrant oscillatory activity patterns at the PPC

Our ECoG *in vivo* recordings unravelled decreased γ amplitude at the PPC in freely moving CPT1C-deficient mice accompanied by unaltered power spectra in the low-frequency bands. Given that γ oscillations

support neural communication between different brain regions (Fell & Axmacher, 2011), these neural network disturbances might interfere with information transmission between the PPC and other interconnected areas, including the hippocampus. Indeed, memory deficits detected in spatial memory tasks, such as the OF habituation and NOL tests, could arise from the disruption of the hippocampus–PPC network activity, given its involvement in the coordinated generation of allocentric and egocentric spatial maps and in episodic memory processing (Moser et al., 2017; Sestieri et al., 2017; Whitlock et al., 2008). In this regard, it is also worth noting that the interactions between θ and γ oscillations give rise to the so-called θ – γ neural code, which is functionally important for cognitive processes including short-term and long-term memory (Lisman & Jensen, 2013). Increases in γ rhythm amplitude along with reduced power of low-frequency oscillations (β and θ) in task-related brain regions have been associated with effective sensory processing and memory formation (Palop & Mucke, 2016). Moreover, experiments in cortical slices showed that LTP was more likely to be induced when pairing extracellular stimulation (fEPSPs) with γ oscillation peaks (Wespatat et al., 2004). Thus, our *in vivo/ex vivo* electrophysiological results allow us to conclude that aberrant network activity at the PPC together with hippocampal plasticity disruption might underlie memory deficits in *CPT1C* KO animals.

CPT1C deficiency causes hippocampus-dependent learning and memory deficits

The hippocampus, especially the CA3–CA1 synapse, is known to be crucial for episodic and visuospatial memory, including different types of associative and non-associative learning (Assini et al., 2009; Broadbent et al., 2004; Gilbert & Brushfield, 2009; Sanchez-Rodriguez et al., 2022; Tsien et al., 1996). Here, we found evidence of multiple hippocampus-dependent memory disruptions associated with *CPT1C* deficiency. Initially, *CPT1C* KO mice exhibited a slight, non-significant habituation to a new environment throughout four OF sessions performed on consecutive days, possibly indicating mild long-term memory deficits. Previously, severe hippocampus-dependent long-term spatial learning impairments have been observed in *CPT1C* KO mice performing the Morris water maze test, possibly caused by alterations of memory acquisition and consolidation associated with *CPT1C* deficiency (Carrasco et al., 2012). In the present study, the NOL task also demonstrated short-term spatial memory deficits 3 h after memory acquisition. In the operant conditioning test, an associative learning task, *CPT1C* KO mice clearly showed slower progression in both training and L/D phases. Interestingly, nearly twice as many WT

animals as *CPT1C* KO mice reached the criterion of the training phase, suggesting that *CPT1C*-mediated regulation of dendritic spine maturation and AMPAR synthesis and trafficking in hippocampal neurons is crucial to sustain plasticity processes involved in learning and memory. Indeed, we observed a significant decrease in the proportion of mature dendritic spines in *CPT1C* KO mice hippocampus, as previously described in *CPT1C*-deficient cultured hippocampal neurons (Carrasco et al., 2012), together with reduced levels of AMPARs and decreased excitatory synaptic transmission (Fado et al., 2015; Gratacos-Batlle et al., 2014). In addition to *CPT1C*-mediated regulation of AMPAR synthesis and trafficking, it is worth noting that the amount of AMPARs is generally lower in immature dendritic spines (Matsuzaki et al., 2004; Petralia et al., 1999). Our data also showed lower total GluA2 protein levels and a decreased ratio of mature to immature GluA2 subunits in the hippocampus of *CPT1C* KO mice, supporting that GluA1/GluA2 AMPAR availability and translocation is hindered, with the latter possibly being explained by the absence of both *CPT1C* depalmitoylating activity and *CPT1C*-mediated inhibition of SAC1 catalytic activity (Casas et al., 2020; Gratacos-Batlle et al., 2018). Importantly, both subunits seem to be required for several phases of LTP, either induction or maintenance, at the hippocampal CA3–CA1 synapse (Romberg et al., 2009). Thus, the effects of *CPT1C* deficiency on AMPAR synthesis and trafficking in the hippocampus might reduce their availability to enable LTP induction and maintenance.

Although HSPs associated with *CPT1C* mutations in humans have not been linked to cognitive alterations to date, the phenotype of *CPT1C* KO mice supports the contention that *CPT1C* loss of function might cause a complicated form of HSP, in which motor dysfunction is accompanied by learning and memory impairments. Given that *CPT1C* variants documented as causative of HSP in humans were heterozygous in all cases reported so far, the homozygous condition of *CPT1C* deficiency in the animals used for this study might explain the inconsistency between observations in humans and mice. Nonetheless, future diagnosis and therapeutic strategies for SPG73 and other *CPT1C*-associated disorders might need to consider the role of the protein in cognition for a better management of the diseases.

Conclusion

Altogether, our work underpins the critical role of *CPT1C* in synaptic plasticity and network activity together with its functional consequences on associative and non-associative learning and memory. Cognitive deficits found here may be explained by impairments in dendritic

spine maturation and reduced synthesis and trafficking of GluA1-containing AMPARs. CPT1C has been proposed as a novel target potentially linking metabolic and neurodegenerative diseases (Spinelli et al., 2017; Virmani et al., 2015). Future studies are necessary to determine its contribution to age-related or pathological cognitive decline (Ding et al., 2021) and, furthermore, its potential as a target for the design of therapeutics.

References

- Assini, F. L., Duzzioni, M., & Takahashi, R. N. (2009). Object location memory in mice: Pharmacological validation and further evidence of hippocampal CA1 participation. *Behavioural Brain Research*, **204**(1), 206–211.
- Bicanski, A., & Burgess, N. (2018). A neural-level model of spatial memory and imagery. *eLife*, **7**, e33752.
- Blackstone, C., O’Kane, C. J., & Reid, E. (2011). Hereditary spastic paraplegias: Membrane traffic and the motor pathway. *Nature Reviews Neuroscience*, **12**(1), 31–42.
- Bliss, T., Collingridge, G. L., Morris, R., & Reymann, K. G. (2018). Long-term potentiation in the hippocampus: Discovery, mechanisms and function. *Neuroforum*, **24**(3), A103–A120.
- Bolivar, V. J., Caldarone, B. J., Reilly, A. A., & Flaherty, L. (2000). Habituation of activity in an open field: A survey of inbred strains and F1 hybrids. *Behavior Genetics*, **30**(4), 285–293.
- Boutry, M., Morais, S., & Stevanin, G. (2019). Update on the genetics of spastic paraplegias. *Current Neurology and Neuroscience Reports*, **19**(4), 18.
- Brechet, A., Buchert, R., Schwenk, J., Boudkazi, S., Zolles, G., Siquier-Pernet, K., Schaber, I., Bildl, W., Saadi, A., Bole-Feysot, C., Nitschke, P., Reis, A., Sticht, H., Al-Sanna’a, N., Rolfs, A., Kulik, A., Schulte, U., Colleaux, L., Abou Jamra, R., & Fakler, B. (2017). AMPA-receptor specific biogenesis complexes control synaptic transmission and intellectual ability. *Nature Communications*, **8**(1), 15910.
- Broadbent, N. J., Squire, L. R., & Clark, R. E. (2004). Spatial memory, recognition memory, and the hippocampus. *PNAS*, **101**(40), 14515–14520.
- Burgess, N., Maguire, E. A., & O’Keefe, J. (2002). The human hippocampus and spatial and episodic memory. *Neuron*, **35**(4), 625–641.
- Carrasco, P., Jacas, J., Sahun, I., Muley, H., Ramirez, S., Puisac, B., Mezquita, P., Pie, J., Dierssen, M., & Casals, N. (2013). Carnitine palmitoyltransferase 1C deficiency causes motor impairment and hypoactivity. *Behavioural Brain Research*, **256**, 291–297.
- Carrasco, P., Sahun, I., McDonald, J., Ramirez, S., Jacas, J., Gratacos, E., Sierra, A. Y., Serra, D., Herrero, L., Acker-Palmer, A., Hegardt, F. G., Dierssen, M., & Casals, N. (2012). Ceramide levels regulated by carnitine palmitoyltransferase 1C control dendritic spine maturation and cognition. *Journal of Biological Chemistry*, **287**(25), 21224–21232.
- Casals, N., Zammit, V., Herrero, L., Fado, R., Rodriguez-Rodriguez, R., & Serra, D. (2016). Carnitine palmitoyltransferase 1C: From cognition to cancer. *Progress in Lipid Research*, **61**, 134–148.
- Casas, M., Fado, R., Dominguez, J. L., Roig, A., Kaku, M., Chohnan, S., Sole, M., Unzeta, M., Minano-Molina, A. J., Rodriguez-Alvarez, J., Dickson, E. J., & Casals, N. (2020). Sensing of nutrients by CPT1C controls SAC1 activity to regulate AMPA receptor trafficking. *Journal of Cell Biology*, **219**(10).
- Chen, N., Pandya, N. J., Koopmans, F., Castelo-Szekelvy, V., van der Schors, R. C., Smit, A. B., & Li, K. W. (2014). Interaction proteomics reveals brain region-specific AMPA receptor complexes. *Journal of Proteome Research*, **13**(12), 5695–5706.
- Cryan, J. E., Mombereau, C., & Vassout, A. (2005). The tail suspension test as a model for assessing antidepressant activity: Review of pharmacological and genetic studies in mice. *Neuroscience and Biobehavioural Reviews*, **29**(4–5), 571–625.
- Dai, Y., Wolfgang, M. J., Cha, S. H., & Lane, M. D. (2007). Localization and effect of ectopic expression of CPT1c in CNS feeding centers. *Biochemical and Biophysical Research Communications*, **359**(3), 469–474.
- Ding, Y., Zhang, H., Liu, Z., Li, Q., Guo, Y., Chen, Y., Chang, Y., & Cui, H. (2021). Carnitine palmitoyltransferase 1 (CPT1) alleviates oxidative stress and apoptosis of hippocampal neuron in response to beta-Amyloid peptide fragment A β 25–35. *Bioengineered*, **12**(1), 5440–5449.
- Djebbari, S., Iborra-Lazaro, G., Temprano-Carazo, S., Sanchez-Rodriguez, I., Nava-Mesa, M. O., Munera, A., Gruart, A., Delgado-Garcia, J. M., Jimenez-Diaz, L., & Navarro-Lopez, J. D. (2021). G-protein-gated inwardly rectifying potassium (Kir3/GIRK) channels govern synaptic plasticity that supports hippocampal-dependent cognitive functions in male mice. *Journal of Neuroscience*, **41**(33), 7086–7102.
- Fado, R., Soto, D., Minano-Molina, A. J., Pozo, M., Carrasco, P., Yefimenko, N., Rodriguez-Alvarez, J., & Casals, N. (2015). Novel regulation of the synthesis of alpha-amino-3-hydroxy-5-methyl-4-isoxazolepropionic acid (AMPA) receptor subunit GluA1 by carnitine palmitoyltransferase 1C (CPT1C) in the hippocampus. *Journal of Biological Chemistry*, **290**(42), 25548–25560.
- Fell, J., & Axmacher, N. (2011). The role of phase synchronization in memory processes. *Nature Reviews Neuroscience*, **12**(2), 105–118.
- Friese, U., Koster, M., Hassler, U., Martens, U., Trujillo-Barreto, N., & Gruber, T. (2013). Successful memory encoding is associated with increased cross-frequency coupling between frontal theta and posterior gamma oscillations in human scalp-recorded EEG. *Neuroimage*, **66**, 642–647.
- Furuya, S., Mitoma, J., Makino, A., & Hirabayashi, Y. (1998). Ceramide and its interconvertible metabolite sphingosine function as indispensable lipid factors involved in survival and dendritic differentiation of cerebellar Purkinje cells. *Journal of Neurochemistry*, **71**(1), 366–377.

- Gilbert, P. E., & Brushfield, A. M. (2009). The role of the CA3 hippocampal subregion in spatial memory: a process oriented behavioural assessment. *Progress in Neuro-Psychopharmacology & Biological Psychiatry*, **33**(5), 774–781.
- Grasselli, G., & Hansel, C. (2014). Cerebellar long-term potentiation: cellular mechanisms and role in learning. *International Review of Neurobiology*, **117**, 39–51.
- Gratacos-Batlle, E., Olivella, M., Sanchez-Fernandez, N., Yefimenko, N., Miguez-Cabello, F., Fado, R., Casals, N., Gasull, X., Ambrosio, S., & Soto, D. (2018). Mechanisms of CPT1C-Dependent AMPAR Trafficking Enhancement. *Frontiers in Molecular Neuroscience*, **11**, 275.
- Gratacos-Batlle, E., Yefimenko, N., Cascos-Garcia, H., & Soto, D. (2014). AMPAR interacting protein CPT1C enhances surface expression of GluA1-containing receptors. *Frontiers in Cellular Neuroscience*, **8**, 469.
- Greger, I. H., Khatri, L., & Ziff, E. B. (2002). RNA editing at arg607 controls AMPA receptor exit from the endoplasmic reticulum. *Neuron*, **34**(5), 759–772.
- Greger, I. H., Watson, J. F., & Cull-Candy, S. G. (2017). Structural and Functional Architecture of AMPA-Type Glutamate Receptors and Their Auxiliary Proteins. *Neuron*, **94**(4), 713–730.
- Gulbins, E., Palmada, M., Reichel, M., Luth, A., Bohmer, C., Amato, D., Muller, C. P., Tischbirek, C. H., Groemer, T. W., Tabatabai, G., Becker, K. A., Tripal, P., Staedtler, S., Ackermann, T. F., van Brederode, J., Alzheimer, C., Weller, M., Lang, U. E., Kleuser, B., ... Kornhuber, J. (2013). Acid sphingomyelinase-ceramide system mediates effects of antidepressant drugs. *Nature Medicine*, **19**(7), 934–938.
- Herring, B. E., & Nicoll, R. A. (2016). Long-Term Potentiation: From CaMKII to AMPA Receptor Trafficking. *Annual Review of Physiology*, **78**(1), 351–365.
- Hong, D., Cong, L., Zhong, S., Liu, L., Xu, Y., & Zhang, J. (2019). A novel CPT1C variant causes pure hereditary spastic paraplegia with benign clinical course. *Annals of Clinical and Translational Neurology*, **6**(3), 610–614.
- Irie, F., & Hirabayashi, Y. (1999). Ceramide prevents motoneuronal cell death through inhibition of oxidative signal. *Neuroscience Research*, **35**(2), 135–144.
- Kakegawa, W., & Yuzaki, M. (2005). A mechanism underlying AMPA receptor trafficking during cerebellar long-term potentiation. *PNAS*, **102**(49), 17846–17851.
- Kaluff, A. V., & Tuohimaa, P. (2005). Mouse grooming microstructure is a reliable anxiety marker bidirectionally sensitive to GABAergic drugs. *European Journal of Pharmacology*, **508**(1–3), 147–153.
- Kamalova, A., & Nakagawa, T. (2021). AMPA receptor structure and auxiliary subunits. *The Journal of Physiology*, **599**(2), 453–469.
- Kida, H., & Mitsushima, D. (2018). Mechanisms of motor learning mediated by synaptic plasticity in rat primary motor cortex. *Neuroscience Research*, **128**, 14–18.
- Leussis, M. P., & Bolivar, V. J. (2006). Habituation in rodents: a review of behavior, neurobiology, and genetics. *Neuroscience and Biobehavioural Reviews*, **30**(7), 1045–1064.
- Lisman, J. E., & Jensen, O. (2013). The theta-gamma neural code. *Neuron*, **77**(6), 1002–1016.
- Matsuzaki, M., Honkura, N., Ellis-Davies, G. C., & Kasai, H. (2004). Structural basis of long-term potentiation in single dendritic spines. *Nature*, **429**(6993), 761–766.
- McKinney, R. A. (2010). Excitatory amino acid involvement in dendritic spine formation, maintenance and remodelling. *The Journal of Physiology*, **588**(1), 107–116.
- Moser, E. I., Moser, M. B., & McNaughton, B. L. (2017). Spatial representation in the hippocampal formation: A history. *Nature Neuroscience*, **20**(11), 1448–1464.
- Padmashri, R., Reiner, B. C., Suresh, A., Spartz, E., & Dunaevsky, A. (2013). Altered structural and functional synaptic plasticity with motor skill learning in a mouse model of fragile X syndrome. *Journal of Neuroscience*, **33**(50), 19715–19723.
- Palomo-Guerrero, M., Fado, R., Casas, M., Perez-Montero, M., Baena, M., Helmer, P. O., Dominguez, J. L., Roig, A., Serra, D., Hayen, H., Stenmark, H., Raiborg, C., & Casals, N. (2019). Sensing of nutrients by CPT1C regulates late endosome/lysosome anterograde transport and axon growth. *Elife*, **8**, e51063.
- Palop, J. J., Chin, J., & Mucke, L. (2006). A network dysfunction perspective on neurodegenerative diseases. *Nature*, **443**(7113), 768–773.
- Palop, J. J., & Mucke, L. (2016). Network abnormalities and interneuron dysfunction in Alzheimer disease. *Nature Reviews Neuroscience*, **17**(12), 777–792.
- Paxinos, G., & Franklin, K. B. (2001). *The Mouse Brain in Stereotaxic Coordinates*. Academic Press, London.
- Petralia, R. S., Esteban, J. A., Wang, Y. X., Partridge, J. G., Zhao, H. M., Wenthold, R. J., & Malinow, R. (1999). Selective acquisition of AMPA receptors over postnatal development suggests a molecular basis for silent synapses. *Nature Neuroscience*, **2**(1), 31–36.
- Pozo, M., Rodriguez-Rodriguez, R., Ramirez, S., Seoane-Collazo, P., Lopez, M., Serra, D., Herrero, L., & Casals, N. (2017). Hypothalamic Regulation of Liver and Muscle Nutrient Partitioning by Brain-Specific Carnitine Palmitoyltransferase 1C in Male Mice. *Endocrinology*, **158**(7), 2226–2238.
- Prut, L., & Belzung, C. (2003). The open field as a paradigm to measure the effects of drugs on anxiety-like behaviors: a review. *European Journal of Pharmacology*, **463**(1–3), 3–33.
- Radosevic, M., Planaguma, J., Mannara, F., Mellado, A., Aguilar, E., Sabater, L., Landa, J., Garcia-Serra, A., Maudes, E., Gasull, X., Lewis, M., & Dalmau, J. (2022). Allosteric Modulation of NMDARs Reverses Patients' Autoantibody Effects in Mice. *Neurol Neuroimmunol Neuroinflamm*, **9**(1), e1122.
- Rinaldi, C., Schmidt, T., Situ, A. J., Johnson, J. O., Lee, P. R., Chen, K. L., Bott, L. C., Fado, R., Harmison, G. H., Parodi, S., Grunseich, C., Rennoise, B., Biesecker, L. G., De Michele, G., Santorelli, F. M., Filla, A., Stevanin, G., Durr, A., Brice, A., ... Fischbeck, K. H. (2015). Mutation in CPT1C Associated With Pure Autosomal Dominant Spastic Paraplegia. *JAMA neurology*, **72**(5), 561–570.
- Risher, W. C., Ustunkaya, T., Singh Alvarado, J., & Eroglu, C. (2014). Rapid Golgi analysis method for efficient and unbiased classification of dendritic spines. *PLoS ONE*, **9**(9), e107591.

- Romberg, C., Raffel, J., Martin, L., Sprengel, R., Seeburg, P. H., Rawlins, J. N., Bannerman, D. M., & Paulsen, O. (2009). Induction and expression of GluA1 (GluR-A)-independent LTP in the hippocampus. *European Journal of Neuroscience*, **29**(6), 1141–1152.
- Roth, R. H., Cudmore, R. H., Tan, H. L., Hong, I., Zhang, Y., & Haganir, R. L. (2020). Cortical Synaptic AMPA Receptor Plasticity during Motor Learning. *Neuron*, **105**(5), 895–908. e895.
- Sanchez-Rodriguez, I., Djebbari, S., Temprano-Carazo, S., Vega-Avelaira, D., Jimenez-Herrera, R., Iborra-Lazaro, G., Yajeya, J., Jimenez-Diaz, L., & Navarro-Lopez, J. D. (2020). Hippocampal long-term synaptic depression and memory deficits induced in early amyloidopathy are prevented by enhancing G-protein-gated inwardly rectifying potassium channel activity. *Journal of Neurochemistry*, **153**(3), 362–376.
- Sanchez-Rodriguez, I., Temprano-Carazo, S., Jeremic, D., Delgado-Garcia, J. M., Gruart, A., Navarro-Lopez, J. D., & Jimenez-Diaz, L. (2022). Recognition Memory Induces Natural LTP-like Hippocampal Synaptic Excitation and Inhibition. *International Journal of Molecular Sciences*, **23**(18), 10806.
- Sanchez-Rodriguez, I., Temprano-Carazo, S., Najera, A., Djebbari, S., Yajeya, J., Gruart, A., Delgado-Garcia, J. M., Jimenez-Diaz, L., & Navarro-Lopez, J. D. (2017). Activation of G-protein-gated inwardly rectifying potassium (Kir3/GirK) channels rescues hippocampal functions in a mouse model of early amyloid-beta pathology. *Scientific Reports*, **7**(1), 14658.
- Sans, N., Racca, C., Petralia, R. S., Wang, Y. X., McCallum, J., & Wenthold, R. J. (2001). Synapse-associated protein 97 selectively associates with a subset of AMPA receptors early in their biosynthetic pathway. *Journal of Neuroscience*, **21**(19), 7506–7516.
- Schwenk, J., Boudkazi, S., Kocylowski, M. K., Brechet, A., Zolles, G., Bus, T., Costa, K., Kollewe, A., Jordan, J., Bank, J., Bildl, W., Sprengel, R., Kulik, A., Roeper, J., Schulte, U., & Fakler, B. (2019). An ER Assembly Line of AMPA-Receptors Controls Excitatory Neurotransmission and Its Plasticity. *Neuron*, **104**(4), 680–692. e689.
- Schwenk, J., Harmel, N., Brechet, A., Zolles, G., Berkefeld, H., Muller, C. S., Bildl, W., Baehrens, D., Huber, B., Kulik, A., Klocker, N., Schulte, U., & Fakler, B. (2012). High-resolution proteomics unravel architecture and molecular diversity of native AMPA receptor complexes. *Neuron*, **74**(4), 621–633.
- Sestieri, C., Shulman, G. L., & Corbetta, M. (2017). The contribution of the human posterior parietal cortex to episodic memory. *Nature Reviews Neuroscience*, **18**(3), 183–192.
- Shi, S., Hayashi, Y., Esteban, J. A., & Malinow, R. (2001). Subunit-specific rules governing AMPA receptor trafficking to synapses in hippocampal pyramidal neurons. *Cell*, **105**(3), 331–343.
- Sierra, A. Y., Gratacos, E., Carrasco, P., Clotet, J., Urena, J., Serra, D., Asins, G., Hegardt, F. G., & Casals, N. (2008). CPT1c is localized in endoplasmic reticulum of neurons and has carnitine palmitoyltransferase activity. *Journal of Biological Chemistry*, **283**(11), 6878–6885.
- Spinelli, M., Fusco, S., Mainardi, M., Scala, F., Natale, F., Lapenta, R., Mattera, A., Rinaudo, M., Li Puma, D. D., Ripoli, C., Grassi, A., D'Ascenzo, M., & Grassi, C. (2017). Brain insulin resistance impairs hippocampal synaptic plasticity and memory by increasing GluA1 palmitoylation through FoxO3a. *Nature Communications*, **8**(1), 2009.
- Stewart, M., Lau, P., Banks, G., Bains, R. S., Castroflorio, E., Oliver, P. L., Dixon, C. L., Kruer, M. C., Kullmann, D. M., Acevedo-Arozena, A., Wells, S. E., Corrochano, S., & Nolan, P. M. (2019). Loss of Frrs11 disrupts synaptic AMPA receptor function, and results in neurodevelopmental, motor, cognitive and electrographical abnormalities. *Disease Models & Mechanisms*, **12**(2), dmm036806.
- Tomita, S., Chen, L., Kawasaki, Y., Petralia, R. S., Wenthold, R. J., Nicoll, R. A., & Brecht, D. S. (2003). Functional studies and distribution define a family of transmembrane AMPA receptor regulatory proteins. *Journal of Cell Biology*, **161**(4), 805–816.
- Tsien, J. Z., Huerta, P. T., & Tonegawa, S. (1996). The essential role of hippocampal CA1 NMDA receptor-dependent synaptic plasticity in spatial memory. *Cell*, **87**(7), 1327–1338.
- Tucholski, J., Pinner, A. L., Simmons, M. S., & Meador-Woodruff, J. H. (2014). Evolutionarily conserved pattern of AMPA receptor subunit glycosylation in Mammalian frontal cortex. *PLoS ONE*, **9**(4), e94255.
- Virmani, A., Pinto, L., Bauermann, O., Zerelli, S., Diedenhofen, A., Binienda, Z. K., Ali, S. F., & van der Leij, F. R. (2015). The Carnitine Palmitoyl Transferase (CPT) System and Possible Relevance for Neuropsychiatric and Neurological Conditions. *Molecular Neurobiology*, **52**(2), 826–836.
- Wang, J., Fang, F., Ding, C., Li, J., Wu, Y., Zhang, W., Bao, X., Lv, J., Wang, X., Ren, X. P. N., & Study, G. (2023). Clinical and genetic spectrum of hereditary spastic paraplegia in Chinese children. *Developmental Medicine and Child Neurology*, **65**(3), 416–423.
- Wespatat, V., Tennigkeit, F., & Singer, W. (2004). Phase sensitivity of synaptic modifications in oscillating cells of rat visual cortex. *Journal of Neuroscience*, **24**(41), 9067–9075.
- Whitlock, J. R., Sutherland, R. J., Witter, M. P., Moser, M. B., & Moser, E. I. (2008). Navigating from hippocampus to parietal cortex. *PNAS*, **105**(39), 14755–14762.
- Wolfgang, M. J., & Lane, M. D. (2011). Hypothalamic malonyl-CoA and CPT1c in the treatment of obesity. *Febs Journal*, **278**(4), 552–558.
- Zhao, L., Spassieva, S. D., Jucius, T. J., Shultz, L. D., Shick, H. E., Macklin, W. B., Hannun, Y. A., Obeid, L. M., & Ackerman, S. L. (2011). A deficiency of ceramide biosynthesis causes cerebellar purkinje cell neurodegeneration and lipofuscin accumulation. *Plos Genetics*, **7**(5), e1002063.
- Zoicas, I., Huber, S. E., Kalinichenko, L. S., Gulbins, E., Muller, C. P., & Kornhuber, J. (2020). Ceramides affect alcohol consumption and depressive-like and anxiety-like behavior in a brain region- and ceramide species-specific way in male mice. *Addiction Biology*, **25**(6), e12847.
- Zucker, R. S., & Regehr, W. G. (2002). Short-term synaptic plasticity. *Annual Review of Physiology*, **64**(1), 355–405.

Additional information

Data availability statement

All data supporting the results in the paper are in the paper itself and the supporting information. Raw data and recordings are available in the laboratory from the corresponding authors and will be provided upon reasonable request.

Competing interests

None.

Author contributions

L.J.-D., D.S. and J.D.N.-L. were responsible for conception or design of the work, with help from all authors regarding certain aspects. G.I.L. performed and analysed most experiments. S.D., I.S.R., E.G.B., N.S.F. and M.R. contributed to the experiments shown in Figs 3, 4 and 7. N.C. generated the *CPT1C* KO mouse. All authors analysed and/or interpreted certain parts of the work. G.I.L. drafted the paper, and J.D.N.-L. and L.J.-D. edited the manuscript. All authors edited and discussed the manuscript and the analysis of the data. All authors approved the final version of the manuscript and agree to be accountable for all aspects of the work in ensuring that questions related to the accuracy or integrity of any part of the work are appropriately investigated and resolved. All persons designated as authors qualify for authorship, and all those who qualify for authorship are listed.

Funding

This work was supported by grants funded by MCIN/AEI/10.13039/501100011033 to L.J.-D. and J.D.N.-L. (BFU2017-82494-P and PID2020-115823-GB-I00) and to D.S. (BFU2017-83317-P and PID2020-119932-GB-I00). L.J.-D. and J.D.N.-L. were also supported by SBPLY/21/180501/000150 funded by JCCM/ERDF—a way of making Europe, and D.S. was supported by María de Maeztu MDM-2017-0729 to Institut de Neurociències, Universitat de Barcelona. G.I.-L. held a predoctoral fellowship granted by UCLM/ESF Plan Propio de Investigación Programme.

Acknowledgements

We thank Dr Aida Castellanos for her enlightened comments about the manuscript.

Keywords

CPT1C, *ex vivo*, habituation test, hippocampus, *in vivo*, locomotor activity, long-term potentiation, mouse, novel object location, operant conditioning, oscillatory activity

Supporting information

Additional supporting information can be found online in the Supporting Information section at the end of the HTML view of the article. Supporting information files available:

Statistical Summary Document

Peer Review History

Figure S1